

1 Regional pollen-based Holocene temperature and 2 precipitation patterns depart from the Northern Hemisphere 3 mean trends

4 Ulrike Herzschuh^{1,2,3}, Thomas Böhmer¹, Manuel Chevalier^{4,5}, [Raphaël Hébert¹⁶](#), Anne
5 [Dallmeyer⁶](#)~~Dallmeyer⁵~~, Chenzhi Li^{1,2}, Xianyong Cao^{1,7}, ~~Raphaël Hébert⁴~~, Odile Peyron⁸, Larisa
6 Nazarova^{1,9}, Elena Y. Novenko^{10,11}, Jungjae Park^{12,13}, Natalia A. Rudaya^{14,15}, Frank Schlütz^{16,17},
7 Lyudmila S. Shumilovskikh¹⁷, Pavel E. Tarasov¹⁸, Yongbo Wang¹⁹, Ruilin Wen^{20,21}, Qinghai
8 Xu²², Zhuo Zheng^{23,24}

9 ¹ Alfred Wegener Institute Helmholtz Centre for Polar and Marine Research, Polar Terrestrial
10 Environmental Systems, Telegrafenberg A45, 14473 Potsdam, Germany

11 ² Institute of Environmental Science and Geography, University of Potsdam, Karl-Liebknecht-Str. 24-25,
12 14476 Potsdam, Germany

13 ³ Institute of Biochemistry and Biology, University of Potsdam, Karl-Liebknecht-Str. 24-25, 14476
14 Potsdam, Germany

15 ⁴ Institute of Geosciences, Sect. Meteorology, Rheinische Friedrich-Wilhelms-Universität Bonn, Auf dem
16 Hügel 20, 53121 Bonn, Germany

17 ~~⁵ Max Planck Institute for Meteorology, Bundesstrasse 53, 20146 Hamburg, Germany~~

18 ⁶ Institute of Earth Surface Dynamics IDYST, Faculté des Géosciences et l'Environnement, University
19 of Lausanne, Batiment Géopolis, 1015 Lausanne, Switzerland

20 [⁶ Max Planck Institute for Meteorology, Bundesstrasse 53, 20146 Hamburg, Germany](#)

21 ⁷ Alpine Paleoecology and Human Adaptation Group (ALPHA), State Key Laboratory of Tibetan Plateau
22 Earth System, Resources and Environment (TPESRE), Institute of Tibetan Plateau Research, Chinese
23 Academy of Sciences, 100101 Beijing, China

24 ⁸ Institut des Sciences de l'Evolution de Montpellier, Université de Montpellier, CNRS UMR 5554,
25 Montpellier, France

26 ⁹ Kazan Federal University, Kremlyovskaya str. 18, 420008 Kazan, Russia

27 ¹⁰ Lomonosov Moscow State University, Faculty of Geography, Leniskie gory 1, 119991 Moscow, Russia

28 ¹¹ Department of Quaternary Paleogeography, Institute of Geography Russian Academy of Science,
29 Staromonrtny lane, 29, 119017, Moscow, Russia

30 ¹² Department of Geography, Seoul National University, 1 Gwanak-ro, Gwanak-gu, Seoul, 08826,
31 Republic of Korea

32 ¹³ Institute for Korean Regional Studies, Seoul National University, 1 Gwanak-ro, Gwanak-gu, Seoul,
33 08826, Republic of Korea

34 ¹⁴ PaleoData Lab, Institute of Archaeology and Ethnography, Siberian Branch, Russian Academy of
35 Sciences, Pr. Akademika 36 Lavrentieva 17, 630090 Novosibirsk, Russia

36 ¹⁵ Biological Institute, Tomsk State University, Pr. Lenina, 26, Tomsk, 634050, Russia

37 ¹⁶ Lower Saxony Institute for Historical Coastal Research, D-26382 Wilhelmshaven, Germany

38 ¹⁷ Department of Palynology and Climate Dynamics, Albrecht-von-Haller Institute for Plant Sciences,
39 University of Göttingen, Untere Karspüle 2, 37073 Göttingen, Germany

40 ¹⁸ Freie Universität Berlin, Institute of Geological Sciences, Palaeontology Section, Malteserstrasse 74-
41 100, Building D, 12249 Berlin, Germany

42 ¹⁹ College of Resource Environment and Tourism, Capital Normal University, 105 West 3rd Ring Rd N,
43 100048 Beijing, China

44 ²⁰ Key Laboratory of Cenozoic Geology and Environment, Institute of Geology and Geophysics, Chinese
45 Academy of Sciences, 19 Beitucheng West Road, Chaoyang District, 100029 Beijing, China

46 ²¹ CAS Center for Excellence in Life and Paleoenvironment, 100044 Beijing, China

47 ²² College of Geographical Sciences, Hebei Normal University, 050024 Shijiazhuang, China

48 ²³ Guangdong Key Lab of Geodynamics and Geohazards, School of Earth Sciences and Engineering,
49 Sun Yat-sen University, 519082 Zhuhai, China

50 ²⁴ Southern Marine Science and Engineering Guangdong Laboratory (Zhuhai), 519082 Zhuhai, China

51 *Correspondence to:* Ulrike Herzs Schuh (Ulrike.Herzs Schuh@awi.de)

52

53 **Abstract.** A mismatch between model- and proxy-based Holocene climate change, known as the
54 ‘Holocene conundrum’^{1,2} may partially originate from the poor spatial coverage of climate reconstructions
55 in, for example, Asia, limiting the number of grid-cells for model-data comparisons. Here we investigate
56 hemispheric, latitudinal, and regional mean time-series as well as time-slice anomaly maps of pollen-
57 based reconstructions of mean annual temperature, mean July temperature, and annual precipitation
58 from 19084676 records in the Northern Hemisphere extratropics. Temperature trends show strong
59 latitudinal patterns and differ between (sub-)continents. While the circum-Atlantic regions in Europe and
60 Easterneastern North America show a pronounced Midmid-Holocene temperature maximum,
61 Westernwestern North America shows only weak changes and Asia mostly shows a continuous
62 Holocene temperature increase, ~~but with strong latitudinal differences~~. Likewise, precipitation trends
63 show certain regional peculiarities such as the pronounced Midmid-Holocene precipitation
64 maximumoptimum between 4030 and 5040°N in Asia and Holocene increasing trends in Europe and
65 Westernwestern North America, which can all be linked with Holocene changes of the regional

66 circulation pattern ~~responding~~linked to temperature change. Given a background of strong regional
67 heterogeneity, we conclude that the calculation of global or hemispheric means, which initiated the
68 'Holocene conundrum' debate, should focus more on understanding the spatio-temporal patterns and
69 their regional drivers.

70

71 1 Introduction

72 Previous comparisons of proxy-based reconstructions and simulations of global Holocene climate
73 change have yielded major mismatches, a discrepancy termed the 'Holocene conundrum' (Liu et al.,
74 2014c; ~~Kaufman and Broadman, 2023~~). While simulations indicate an increase in Holocene
75 temperature (Liu et al., 2014c), proxy data syntheses rather support a ~~Mid~~mid-Holocene ~~temperature~~
76 ~~maximum~~optimum (Marcott et al., 2013; Kaufman et al., 2020b). Recently, several explanations for this
77 finding were proposed, most of which assign the mismatch to biases in the proxy data with respect to
78 location or seasonality (Marsicek et al., 2018; Bader et al., 2020; Bova et al., 2021; Osman et al., 2021).

79 Previous temperature reconstructions from continental areas are mainly available from the circum-North
80 Atlantic region, and are potentially unrepresentative of the whole Northern Hemisphere temperature
81 change, as the region was strongly impacted by the vanishing Laurentide ice-sheet (Rolandone et al.,
82 2003; Chouinard and Mareschal, 2009). Synthesis studies hitherto included ~~rather only a~~ few records
83 from the large non-glaciated Asian continent (~~Andreev et al., 2004; Leipe et al., 2015; Melles et al., 2012;~~
84 ~~Nakagawa et al., 2002; Stebich et al., 2015; Tarasov et al., 2009 and 2013~~). ~~The inclusion despite the~~
85 ~~existence of recently compiled~~many Holocene pollen records (Cao et al., 2019; Herzschuh et al., 2019)
86 and high-quality modern pollen datasets (Tarasov et al., 2011; Cao et al., 2014; Davis et al., 2020;
87 Dugerdil et al., 2021) ~~from Asia now allows~~potentially ~~allowing~~ for higher quality quantitative
88 reconstructions.

89 While temperature patterns have often been studied, hemispheric syntheses of quantitative precipitation
90 change during the Holocene are not yet available. A recent study of qualitative moisture proxy data
91 suggests an overall warm and dry ~~Mid~~mid-Holocene in the Northern Hemisphere mid-latitudes, related
92 to the weakened latitudinal temperature gradient (Routson et al., 2019). This trend contrasts with the
93 idea of positive hydrological sensitivity, that is, warm climates are wet at a global scale (Trenberth, 2011),
94 which was confirmed from proxy and model studies from monsoonal areas in lower latitudes (Kutzbach,
95 1981; Wang et al., 2017). ~~However, the~~The study of Routson et al. (2019) only included a few records
96 from the subtropical monsoonal Asia that is known for complex Holocene moisture patterns (Herzschuh,
97 2004; Chen et al., 2019; Herzschuh et al., 2019). These and further synthesis studies (Wang et al., 2010;
98 Chen et al., 2015; Wang et al., 2020) also gave a plethora of alternative explanations to characterize
99 these patterns, including interactions between the monsoon and westerlies circulation and evaporation
100 effects.

101 Pollen spectra are a well-established ~~paleoclimate~~proxy and quantitative estimates of
102 past climatic change are mainly derived by applying (transfer functions of) modern pollen-climate
103 calibration sets to fossil pollen records (Birks et al., 2010; Chevalier et al., 2020). Accordingly, pollen-

104 based reconstructions constitute a substantial part of multi-proxy syntheses (e.g., Kaufman et al., 2020b),
105 ~~albeit but unfortunately, they are~~ derived from different calibration sets and methods, ~~which~~
106 ~~makes making~~ a consistent assessment of inherent reconstruction biases difficult. Pollen data are one
107 of the few land-derived proxies available that can theoretically contain independent information on both
108 temperature and precipitation in the same record (Chevalier et al., 2020; Mauri et al., 2015). Consistent
109 pollen-based reconstructions can thus contribute to better characterizing past temperature and
110 precipitation changes across large landmasses and how these changes co-vary over time (Davis et al.,
111 2003).

112 Here, we analyze spatio-temporal patterns of pollen-based reconstructions of mean annual temperature
113 (T_{ann}), mean July temperature (T_{July}), and mean annual precipitation (P_{ann}) from ~~19084676~~ sites from the
114 Northern Hemisphere extratropics that were generated using harmonized methods and calibration
115 datasets (LegacyClimate 1.0, Herzschuh et al., 2022a) and have revised chronologies (Li et al., 2022).
116 We address the following questions: (1) What are the continental, latitudinal, and regional patterns of
117 Holocene temperature change in the Northern Hemisphere extratropics and how do our new
118 reconstructions align with the global averaged trends of a previous global temperature synthesis? (2)
119 What are the continental, latitudinal, and regional patterns of Holocene precipitation change and how
120 do these changes co-vary with temperature trends?

121

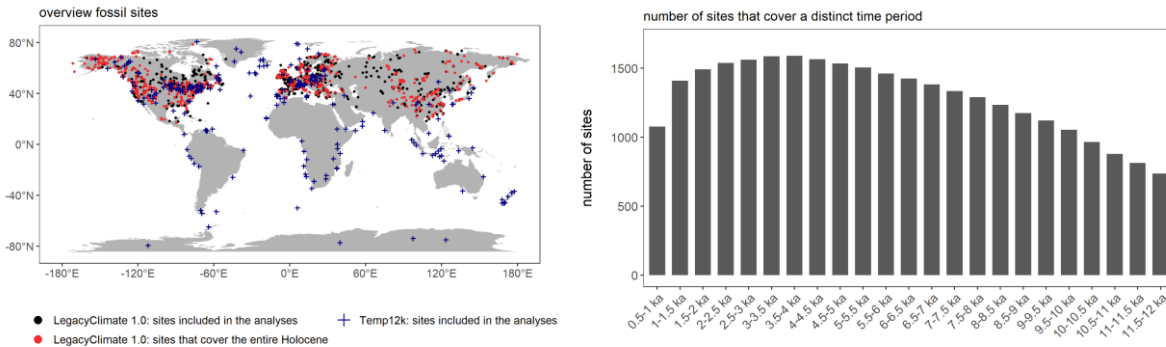
122 2 Methods

123 This study analyzes pollen-based reconstructions provided in the LegacyClimate 1.0 dataset
124 (Herzschuh et al., ~~2021~~2022a). It contains pollen-based reconstructions of T_{July} , T_{ann} , and P_{ann} of
125 ~~25932594~~ records along with transfer function metadata and estimates of reconstruction errors and is
126 accompanied by a manuscript analyzing reconstruction biases and presenting reliability tests
127 (Herzschuh et al., 2022a).- The fossil pollen records, representing the LegacyPollen 1.0 ~~dataset, were~~
128 ~~derived from multiple natural archives, most commonly continuous lacustrine and peat accumulations~~
129 (Herzschuh et al., 2022b), ~~and) dataset,~~ originate from ~~the~~ Neotoma Paleoecology Database
130 ('Neotoma' hereafter; {last access: April 2021; Williams et al., 2018~~July 2020~~), a dataset from
131 ~~Easterneastern~~ and ~~Centralecentral~~ Asia (Cao et al., 2013; Herzschuh et al., 2019), a dataset from
132 ~~Northernnorthern~~ Asia (Cao et al., 2019), and a few additional records to fill up some spatial data gaps
133 in Siberia.

134 -The chronologies of LegacyPollen 1.0 are based on revised 'Bacon' (Blaauw and Christen, 2011) age-
135 depth models with calibrated ages at each depth~~chronologies~~ provided by Li et al. (2022). Taxa are
136 harmonized to genus level for woody ~~taxa~~ and major herbaceous taxa and to family level for other
137 herbaceous taxa. Along with LegacyClimate 1.0, a taxonomically harmonized modern pollen dataset is
138 provided (a total of ~~1537945,344~~ samples; Herzschuh et al., ~~2022a~~2024) which includes datasets from
139 Europe (EMPD2, Davis et al., 2020), Asia (Tarasov et al., 2011; Herzschuh et al., 2019; Dugerdil et al.,
140 2021), and North America (from Neotoma; Whitmore et al., 2005). LegacyClimate 1.0 also provides the

141 climate data for the sites of the modern pollen samples that were derived from WorldClim 2 (Fick and
142 Hijmans, 2017).

143 ~~Of the 2594 records available, 1676 records cover at least 4000 years of the Holocene and were~~
144 ~~included in the time-slice comparisons (Fig. 1). The construction of time-series to estimate the means~~
145 ~~of climate variables was restricted to those 991 records that cover the full period of 11 to 1 ka.~~

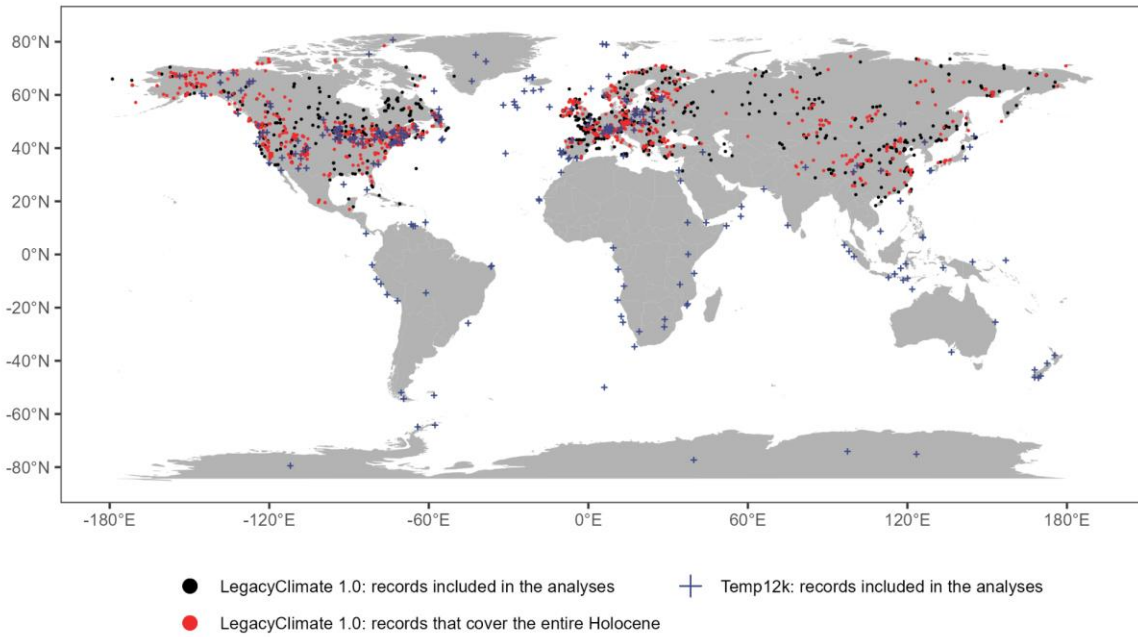


146 **Figure 1. Temporal and spatial coverage of the LegacyClimate1.0 dataset (dots) and of Temp12K**
147 **(Kaufman et al. 2020b, crosses) used in this analysis.** The map shows sites that cover the entire
148 Holocene (i.e., 11-1 ka) as red symbols and those that cover parts of the Holocene but at least 4000
149 years in the period between 0 and 12 ka as black symbols.

151 LegacyClimate 1.0 provides reconstructions based on different methodologies including two versions of
152 WA-PLS (weighted averaging partial least squares regression, a transfer function-based approach) and
153 MAT (modern analogue technique). For each fossil site, we calculated the geographic distance between
154 each modern sampling site and each fossil location and selected a unique calibration set from modern
155 sites within a 2000 km radius was first set up (Cao et al., 2014), as it was shown to be a good trade-off
156 between analog quality and quantity (Cao et al., 2017). For WA-PLS, the used best component,
157 typically first or second, was identified using model statistics as derived from leave-one-out cross-
158 validation based on the criterion that an additional component be used only if it improves the root mean
159 squared error (RMSE) by at least 5% (ter Braak and Juggins, 1993). A WA-PLS_tailored reconstruction
160 set is also provided in the LegacyClimate 1.0 dataset (Herzschuh et al., 2022a), which addresses the
161 problem that co-variation in modern temperature and precipitation data can be transferred into the
162 reconstruction. To reduce the influence of one climate variable on the target variable). In WA-
163 PLS_tailored, the modern range of the non-target variable is reduced by tailoring the modern pollen
164 dataset to a selection of sites with little covariance between the two variables. For example, to
165 reconstruct T_{July} we identified the P_{ann} range reconstructed by WA-PLS and extended it by 25% at both
166 ends. For the selection of sites in the modern training dataset, we then restricted modern P_{ann} to that
167 range accordingly. As such, we keep all information for reconstruction from those modern pollen spectra
168 that cover a wide temperature range but downweight the information from pollen spectra covering a
169 wide precipitation range restrict the impact of precipitation on the temperature reconstruction and vice
170 versa. However, initial assessments did not show any major differences compared to using the standard
171 WA-PLS-derived reconstruction. Therefore As such, we do not make use of this dataset for this study so

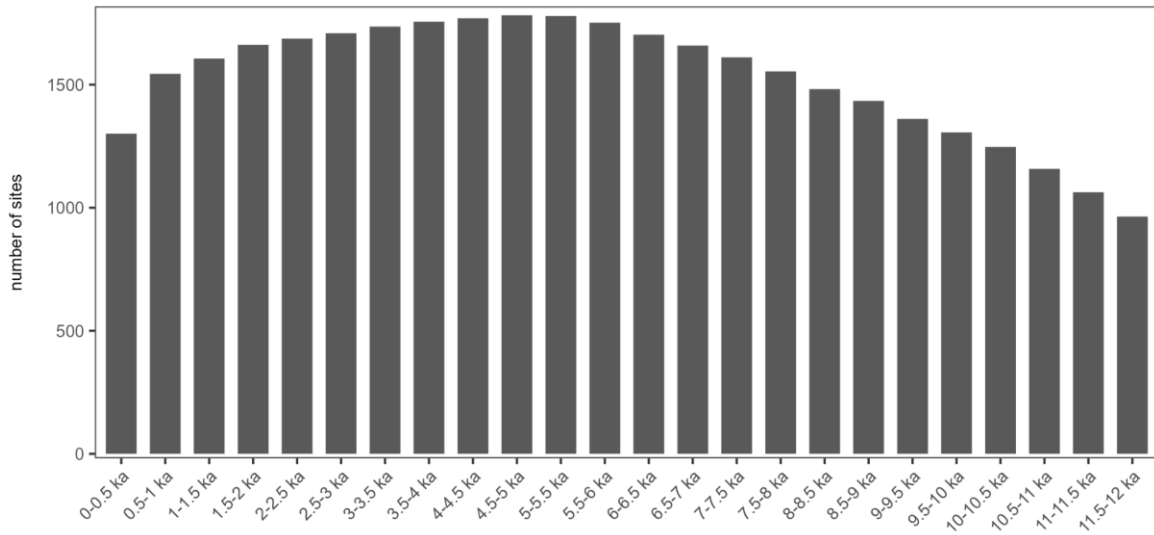
172 as to be consistent with previous studies. For comparison, we provide a plot with hemispheric,
173 continental, and latitudinal mean curves for T_{July} , T_{ann} , and P_{ann} reconstructed by WA-PLS tailored in the
174 supplement. The MAT reconstructions were derived from the seven best analoganalogues that we
175 identified based on the dissimilarity measures between the fossil samples and the modern pollen
176 assemblages using the squared-chord distance metric (Simpson, 2012). MAT reconstructions were
177 highly correlated with those obtained by WA-PLS (Herzschuh et al., 2022a). Here, we opted for the
178 widely used WA-PLS, as it is less sensitive to the size and environmental gradient length of the modern
179 pollen dataset and is thus less affected by spatial autocorrelation effects and can better handle poor
180 analoganalogue situations (ter Braak and Juggins, 1993; Telford and Birks, 2011; Cao et al., 2014;
181 Chevalier et al., 2020). Statistical significance tests sensu Telford & Birks (2011) were performed for
182 each site for WA-PLS, WA-PLS tailored and MAT and assessed in Herzschuh et al. (2022a).
183 Of the 2593 records available in LegacyClimate 1.0, 1908 records with at least 5 samples that cover at
184 least 4000 years of the Holocene and have a The-mean temporal resolution of 1000 years or less were
185 included in the time-slice comparisons based on this criterion (Fig. 1). The construction of time-series
186 to estimate the means of climate variables was further restricted to 957 records that cover the full period
187 of 11 to 1 ka.

LegacyClimate 1.0 and Temp12k datasets | overview



188

Legacy Climate 1.0: number of records that cover a distinct time period



189

190 **Figure 1. (top) Spatial coverage of the LegacyClimate 1.0 (dots) and Temp12k (Kaufman et al.**
 191 **2020b, crosses) datasets used in this analysis.** The map shows sites that cover the entire Holocene
 192 (i.e., 11-1 ka) as red symbols and those that cover parts of the Holocene but at least 4000 years in the
 193 period between 12 and 0 ka as black symbols. (bottom) Temporal coverage of the LegacyClimate 1.0
 194 dataset.

195

196 The mean root mean squared error of prediction (RMSEP; $\sqrt{WA-PLS}$) from all 957994 sites included in
 197 the time-series analyses is $2.448 \pm 0.7^\circ\text{C}$ (one standard deviation) for T_{July} , $2.664 \pm 0.5^\circ\text{C}$ for T_{ann} , and
 198 244 ± 74 242.54 ± 75.5 mm for P_{ann} . They show a spatial pattern in that the RMSEPs are higher in areas

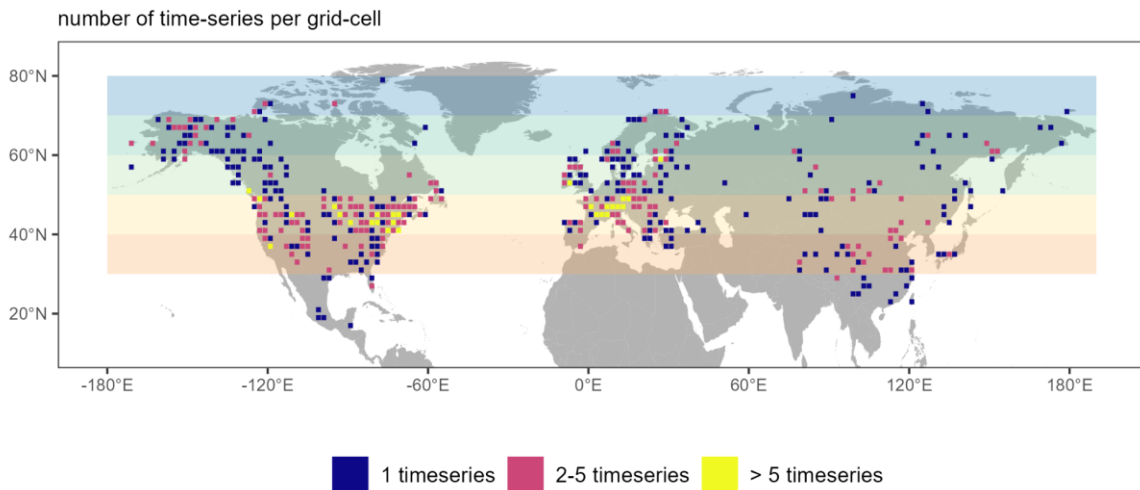
199 with steep climate gradients (e.g. ~~Central-, central~~ Asia and along the western coast of North America);
200 see Fig. 53 in Herzschuh et al., 2022a). As it has already been shown in previous comparisons, WA-
201 PLS can have higher RMSEPs than MAT but these do not necessarily reflect a less reliable
202 reconstruction but methodological differences. MAT is known to be more sensitive to spatial
203 autocorrelation, which causes the model performance to be over-optimistic compared to WA-PLS (Cao
204 et al., 2014). Besides, ~~the reconstruction errors are likely much smaller when only the~~ trends and the
205 relative changes ~~are assessed~~, as interpreted in this study, are less sensitive to methodological biases
206 than absolute values.

207 Derived time-series of T_{July} , T_{ann} , and P_{ann} were smoothed over a 500-yr time-scale and resampled at a
208 100 yr-resolution using the *corit* package in R (version 0.0.0.9000, Reschke et al., 2019). Because the
209 original time-series are unevenly spaced, we used this package as it is designed to resample irregularly
210 sampled time-series to an equidistant spacing (Reschke et al., 2019). The smoothing length of 500
211 years reflects the typical resolution of the original pollen records. These derived time-series were
212 sampled at selected time-slices and converted into a regular $2^\circ \times 2^\circ$ raster grid (by taking the mean of
213 all records located within the grid-cell) using the *raster* package in R (version 3.5-11, R Core Team,
214 2020; Hijmans et al., 2021). ~~P_{ann} is presented as % relative to the 1 ka reference period (mean curve)~~
215 ~~or relative to the younger time-slice (map).~~

216 To calculate zonal, (sub-)continental (i.e., Asia ($>43^\circ E$), Europe ($<43^\circ E$), Eastern North America
217 ($<104^\circ W$; Williams et al., 2000) and Western North America), and hemispheric means we selected all
218 ~~957994~~ smoothed and resampled time-series of T_{July} , T_{ann} , and P_{ann} that cover the full period between
219 11 and 1 ka and calculated climate anomalies for all three climate variables. Rather than using the
220 anomalies for P_{ann} we calculated the precipitation change as % relative to the 1 ka reference period (Fig.
221 3) or relative to the younger time-slice (Fig. 4), converted them into a regular $2^\circ \times 2^\circ$ raster grid. In total,
222 437 grid-cells between 30 and $80^\circ N$ are covered by one or more time-series. The estimate at 1 ka was
223 used as a reference to calculate the anomalies, as many records either poorly or do not cover the last
224 0.5 ka. Weights proportional to the inverse number of time-series per cell in the grid were used to
225 calculate the weighted ~~The mean~~ and standard deviation (using the *wtd.mean* and *wtd.var* functions
226 from the *Hmisc* R-package, version 5.0-1, Harrell & Dupont, 2023). The weighted standard error was
227 calculated by dividing the weighted standard deviation estimates by the square root of climate variable
228 anomalies of the number of grid cells with at least 1 record. In total, 436 all-grid cells between $17^\circ N$ and
229 $79^\circ N$ are covered by one or more time-series (Fig. 2).

230 ~~The cell curves originating from a zonal mean overband of 10° bands of (a-sub-)continents-continent~~
231 ~~(e.g., for 30 - $40^\circ N$ of Europe) were calculated and also used to derive the zonal mean time-series for~~
232 ~~each sub-continent. Such derived zonal means were weighted by the terrestrial area represented in the~~
233 ~~zonal band to calculate the mean time-series of the (sub-)continents, with weights proportional to the~~
234 ~~terrestrial area in a zonal band based on the WGS84 EASE-Grid 2.0 global projection (Brodzik et al.,~~
235 ~~2012), i.e., Asia, Europe, Eastern North America ($<105^\circ W$; Williams et al., 2000).~~ Likewise, the area-
236 weighting was applied to derive the continental means and hemispheric-wide (zonal) means. We
237 compare the linear trends of all zonal means with each other for each continent, as well as the linear

238 trends of the continental weighted means, taking into account the standard error of each average. We
 239 take a Monte-Carlo approach to generate ensembles of trend estimates after adding random errors and
 240 use a standard t-test to assess, pairwise, whether the means of the ensembles are significantly
 241 different. Area calculation was implemented using the *raster* package in R (version 3.5-11, R Core Team,
 242 2020; Hijmans et al., 2021).



243 **Figure 2. Number of time-series per grid cell.** The map shows the number of time-series that are
 244 merged into one grid cell. Colored rectangles (as used for the zonal mean curves in Fig. 3) indicate the
 245 latitudinal band a respective grid cell belongs to.
 246

247
 248 Furthermore, we extracted ~~325~~~~the~~~~249~~ records that cover the full Holocene period in the Temp12k
 249 dataset ([version 1-1-0; https://lipdverse.org/project/temp12k](https://lipdverse.org/project/temp12k), last access February 2023; Kaufman et al.,
 250 2020b) applying the same restrictions as with the LegacyClimate 1.0 dataset (i.e., at least 5 samples, a
 251 mean temporal resolution of 1000 years or less). ~~Instead;~~~~instead~~ of 11.0 ka we here used a cut-off of
 252 10.5 ka as many records in this dataset start shortly after 11.0 ka). ~~For 43 sites, more than one~~
 253 ~~temperature time-series ; Fig. 1).~~ ~~Four records were stored in the Temp12k dataset. In these cases, we~~
 254 ~~selected that time-series with the least amount~~~~deleted because~~ of missing temperature values in the
 255 ~~period between 10.5 and 1 ka, extreme Holocene deviations of >7°C~~ leaving 272245 records that were
 256 used to construct the mean temperature anomaly time-series similar to the approach described for the
 257 LegacyClimate 1.0 dataset. We excluded all pollen-based reconstructions from the
 258 Temp12k dataset (~~n=111~~) which are between 30°N and 80°N (~~n=117~~) and which are already present in
 259 the LegacyClimate 1.0 dataset to avoid duplications with the LegacyClimate 1.0 dataset when
 260 integrating both datasets into a joint hemispheric and global mean temperature stack curve.

261
 262
 263

264 3 Results

265 3.1 Spatio-temporal pattern of temperature reconstructions

266 The temporal patterns of temperature records covering the entire Holocene (i.e., 11-1 ka) show strong
267 differences between continents (Fig. 32). Europe shows a pronounced ~~Midmid-Holocene temperature~~
268 ~~maximum optimum~~ of $+1.3 \pm 0.431^\circ\text{C}$ for T_{July} at 5.7-2 ka while the T_{ann} ~~maximum optimum occurs later~~
269 ~~and~~ is less pronounced ($+0.9 \pm 0.487^\circ\text{C}$ at 5.86 ka). The ~~Midmid-Holocene~~ T_{July} was weaker ~~and occurred~~
270 ~~earlier~~ in Eastern North America ($+0.5 \pm 0.249^\circ\text{C}$ at 7.0 ka) while T_{ann} warming was ~~in a similar range~~
271 $+0.7 \pm 0.385^\circ\text{C}$ ~~at the same time period (7.0 ka).~~ ~~(T_{ann}) to Europe.~~ Asia (T_{July}) and Western North America
272 (T_{ann}) show almost no ~~maximum optimum~~ but only some variations around a continuously increasing
273 Holocene trend, with a higher increase rate before 6 ka than after 6 ka.

274 Aside from these differences among (sub-)continents, certain regional differences exist. Early Holocene
275 cold climate anomalies were most pronounced in latitudes between 45°N and 65°N , particularly in
276 Northern Europe, Northeastern Asia, and Alaska (Fig. 43) with above 2.5°C deviation to ~~mean-Holocene~~
277 T_{ann} ~~maximum optimum~~ values in most records. The most pronounced T_{ann} ~~maximum (more than~~
278 ~~optimum of $>+1.5^\circ\text{C}$ warmer than compared to the Late late Holocene)~~ can be found in Europe north of
279 60°N and Eastern North America between 60°N and 70°N , forming a circum-North Atlantic pattern (Fig.
280 54). Records from Eastern Europe, inner Asia, and Southern North America show mostly no ~~Midmid-~~
281 ~~Holocene temperature maximum optimum~~, but rather a ~~Late late-Holocene maximum optimum~~. Records
282 with an ~~Early early-Holocene maximum optimum~~ dominate the north-central part of North America and
283 China, though these areas are characterized by high spatial variability. High ranges of Holocene
284 temperature variations (~~larger than $>5^\circ\text{C}$~~) are found in mid-latitude Europe, Western Canada,
285 Southeastern US, and along the north Asian Pacific coast.

286 The averaged Northern Hemisphere ~~north of $>30^\circ\text{N}$~~ time-series of all records that cover the entire
287 Holocene ($n=991$, Fig. 35) indicate that mean T_{July} was lowest at the beginning of the Holocene ($-$
288 $0.7 \pm 0.259^\circ\text{C}$ compared to present), increased until 7 ka ($+0.5 \pm 0.147^\circ\text{C}$ compared to present), and
289 slightly decreased afterwards to reach modern temperatures. T_{ann} was also lowest at the beginning of
290 the Holocene ($-1.4 \pm 0.226^\circ\text{C}$ compared to present) and reached its maximum of $0.3 \pm 0.229^\circ\text{C}$ compared
291 to present at 6.54 ka.

292 Finally, our revised global temperature curve includes all of our records ~~and those of that cover the entire~~
293 ~~Holocene plus all records in~~ the Temp12k dataset (Kaufman et al., 2020b) that cover the entire Holocene
294 ~~(in total, excluding duplicate and are not from identical pollen records, 1098 (in total, 1129 records).~~ It
295 shows that mean T_{ann} was lowest during the ~~Early early~~ Holocene at 10.53 ka with a $-0.3 \pm 0.3007^\circ\text{C}$
296 anomaly relative to 1 ka and warmest at 6.65-4 ka with a warming of $0.3 \pm 0.349^\circ\text{C}$. For ~~the~~ Northern
297 Hemisphere extratropics ($30-80^\circ\text{N}$), we find that mean T_{ann} was lowest during the ~~Early early~~ Holocene
298 at 10.5 ka with a $-0.3 \pm 0.122^\circ\text{C}$ anomaly relative to 1 ka and warmest at 6.4 ka with a warming of
299 $0.08 \pm 0.04^\circ\text{C}$.

300 ~~The linear trends of all zonal means are significantly different ($p < 0.01$) for both T_{July} (Appendix Table~~
301 ~~2) and T_{ann} (Appendix Table 3). While the uncertainty range is small in the mid-latitudes they are larger~~

302 for the 30-40°N zonal band (T_{July}) and especially for the polar region (T_{July} and T_{ann} ; Appendix Fig. 3).
303 The linear trends for T_{July} for all continental means are significantly different, despite overlapping
304 uncertainty ranges for several zonal bands, e.g. 40-50°N and 50-60°N in Western North America
305 (Appendix Fig. 4); 30-40°N and 50-60°N in Eastern North America (Appendix Fig. 5), 30-40°N and 40-
306 50°N, as well as 50-60°N and 60-70°N in Asia (Appendix Fig. 7). Large uncertainty ranges can be found
307 in the 30-40°N zonal band (Europe, Appendix Fig. 6) and the polar region (Western North America,
308 Appendix Fig. 4; Asia, Appendix Fig. 7). The linear trends for T_{ann} reveal similarities between the
309 weighted means of Europe and Asia (Europe vs. Asia: $p = 0.08$; Asia vs. Europe: $p = 0.9$; Appendix
310 Table 5). For overlapping uncertainty ranges similar patterns compared to those of T_{July} can be found,
311 except for Eastern North America, where the zonal means of 30-40°N and 50-60°N are very different to
312 each other, especially in the Early and Mid-Holocene (Appendix Fig. 5). Similar to T_{July} , the largest
313 uncertainty ranges can be found either in the 30-40°N or the 70-80°N zonal bands. For the weighted
314 continental means the uncertainty ranges of Western and Eastern North America show a strong overlap,
315 i.e. the T_{July} mean of Eastern North America mirrors the weighted Northern Hemisphere T_{July} mean. T_{July}
316 in Asia is lower overall while in Europe it is higher overall than the Northern Hemispheric mean, but the
317 uncertainty range of both continental means are larger than those in North America (West and East)
318 and the Northern Hemisphere. For T_{ann} the uncertainty ranges in all continents show a stronger overlap
319 than for T_{July} with pronounced differences between the Western and the Eastern part of North America
320 (Appendix Fig. 8).

322 3.2 Spatio-temporal pattern of precipitation reconstructions

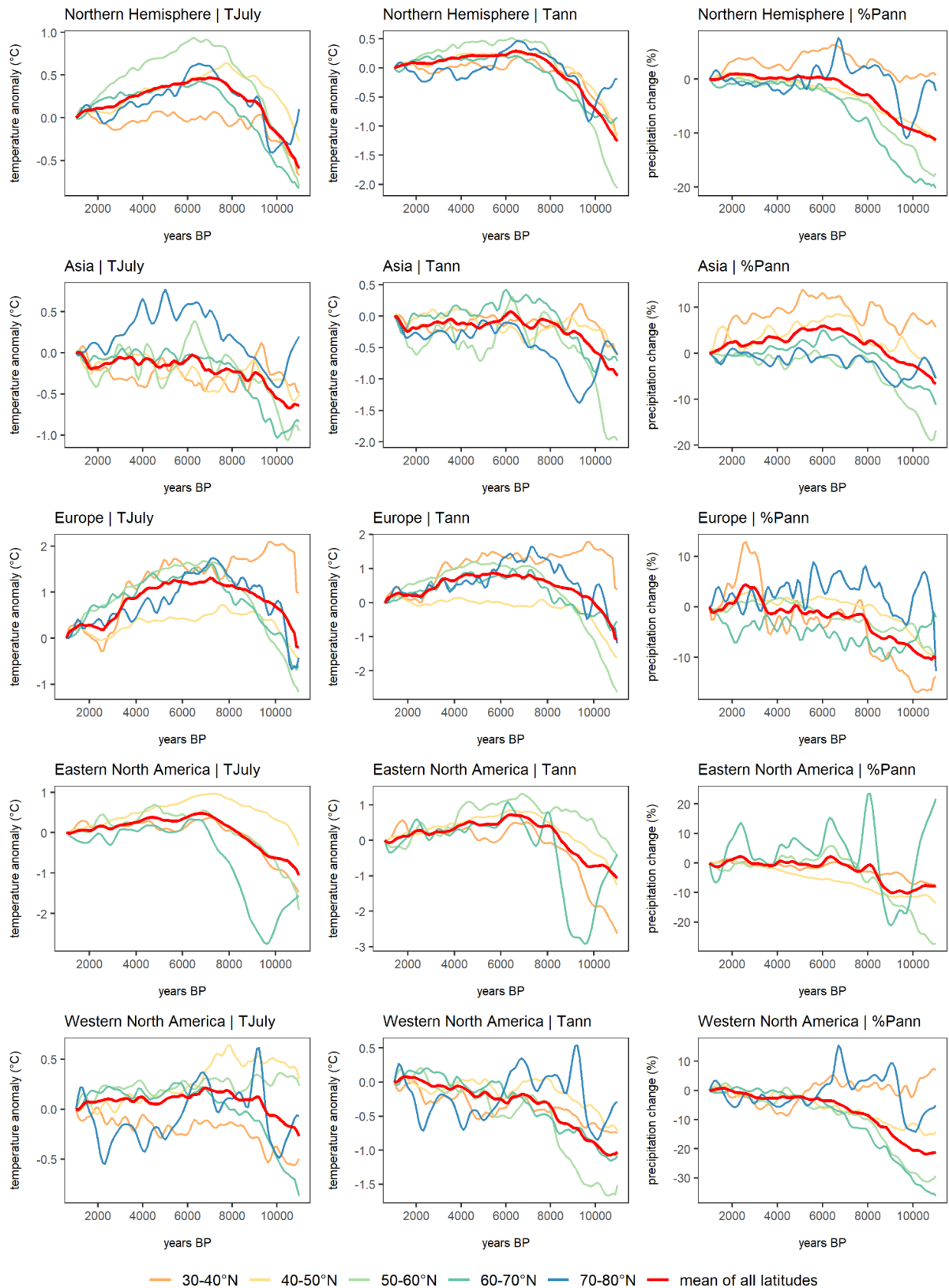
323 Holocene mean P_{ann} variations (as % of modern value) averaged across the Northern Hemisphere
324 extratropics have patterns that are mostly similar to T_{ann} with P_{ann} being lowest during the Early Holocene
325 ($-11.6 \pm 2.825\%$ at 11 ka compared to 1 ka) and increasing until 6.5.9 ka before becoming relatively stable
326 (Fig. 32).

327 In contrast to the averaged Northern Hemisphere pattern, the (sub-)continental precipitation patterns
328 differ from their respective temperature patterns. The mean precipitation time-series of Western North
329 America and Europe increases from the Earlyearly Holocene to the Latelate Holocene; averaged
330 Eastern North America precipitation increased until 6.5 ka and varies slightly around modern values
331 from then; and Asia shows a pronounced maximum between 7 and 5 ka.

332 Time-series maps of latitudinal means and differences (Fig. 43) reveal strong spatial patterns,
333 particularly for Asia. The latitudinal mean time-series in Asia show a strong increase toward the Midmid-
334 Holocene of mostly $>10\%$. After ca. 7 ka, certain differences exist: while the 70°N mean shows no clear
335 further trend, the other mean curves show a precipitation maximuman optimum which is at least 5%
336 above the Late late-Holocene minimum. Precipitation maximaoptima (compared with the Latelate
337 Holocene) are more pronounced and occur later at lower latitudes. Furthermore, the 6-1 ka difference
338 maps reveal that the Midmid-Holocene moisture maximum in subtropical Asia was most pronounced in

339 ~~East~~east-central China with many records even showing \geq 50% higher values at 6 ka compared to 1
340 ka (Fig. 43).

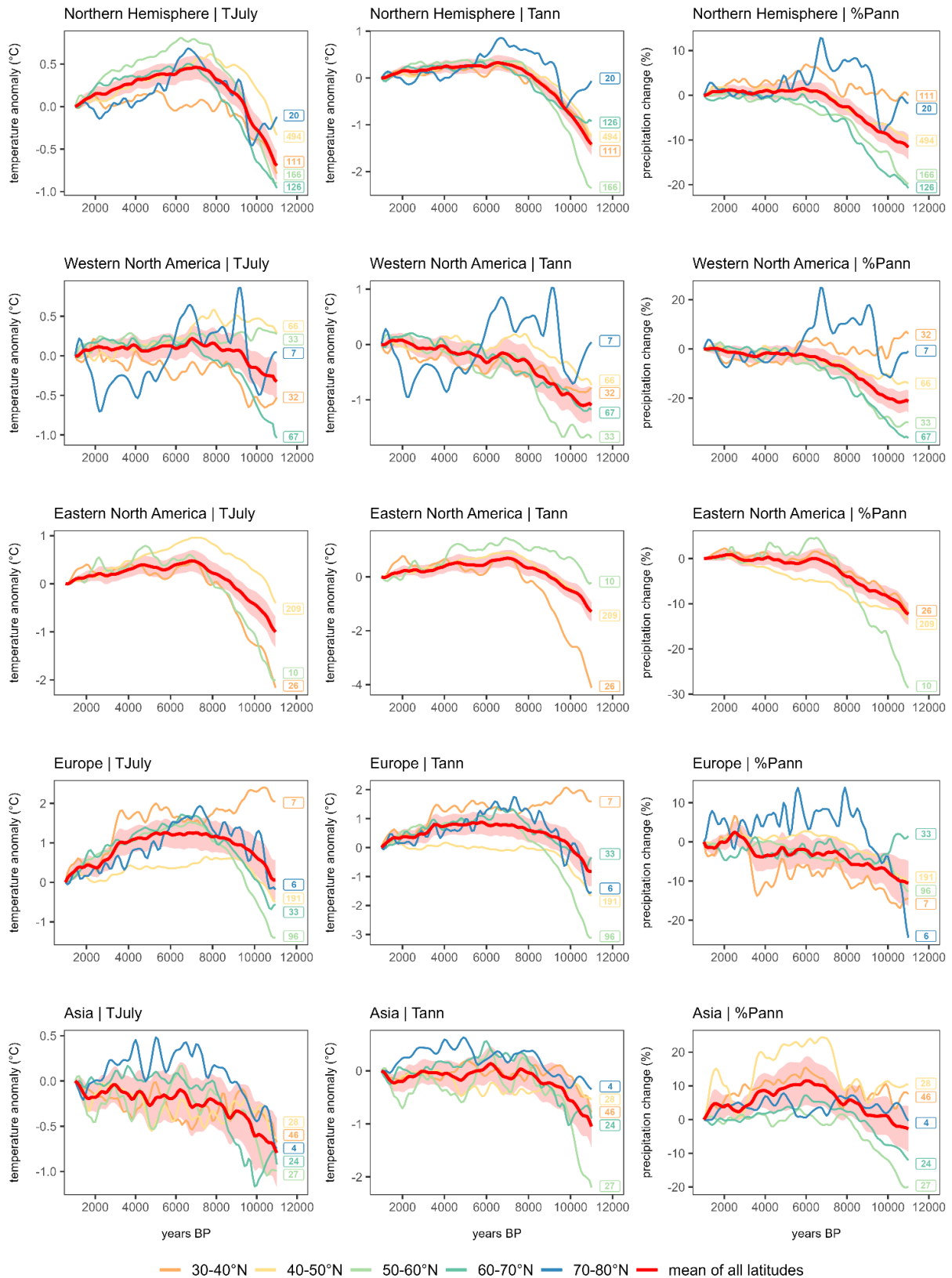
341 The Holocene precipitation increase in the other (sub-)continents is particularly strong in the 30-40°N
342 bands in subtropical Europe and mid-latitude North America with >13% and >20% precipitation increase,
343 respectively. In Europe and Western and Eastern North America the records from 70-80°N show an
344 ~~Early~~ early-Holocene precipitation maximum (particularly pronounced in Alaska), which is in contrast to
345 the trends in almost all other latitudinal bands.



346

347 **Figure 2.** Comparing the linear trends for all zonal means reveals significant differences in all zonal
 348 bands for Europe and Eastern North America ($p < 0.01$). Similarities in the trends can be found in
 349 Western North America (70-80°N vs. 30-40°N: $p = 0.06$) and especially in Asia, where several

350 combinations of zonal trends are not significantly different (i.e. 30-40°N vs. 40-50°N ($p = 0.08$) and 30-
351 40°N vs. 70-80°N ($p = 0.76$)). For details, see Appendix Table 4. All trends in the continental precipitation
352 means are found to be different ($p < 0.01$; Appendix Table 5). The uncertainty ranges for all latitudinal
353 means are small, except for the 70-80°N zonal band in the polar region ($\%P_{ann}$; Appendix Fig. 3). In
354 Western North America the zonal means of 50-60°N and 60-70°N show a strong overlap in their
355 uncertainty ranges and the largest uncertainty range can be found in the polar region (Appendix Fig.4).
356 In Europe and Asia, the mid-latitudes show the smallest uncertainty ranges, while the southernmost and
357 northernmost zonal bands have higher uncertainty ranges (Appendix Fig. 6 and 7). Notable is the 40-
358 50°N zonal band in Asia, which shows the highest uncertainty range of all continental zonal bands,
359 especially in the Mid-Holocene (Appendix Fig. 7). Compared to the Northern Hemispheric mean, the
360 continental $\%P_{ann}$ mean of Eastern North America shows the smallest deviations, although the
361 continental mean only comprises the zonal bands between 30°N and 60°N. Precipitation changes in
362 Western North America are overall lower than the Northern Hemispheric mean, while the precipitation
363 changes in Asia are overall higher (Appendix Fig. 8).



364

365

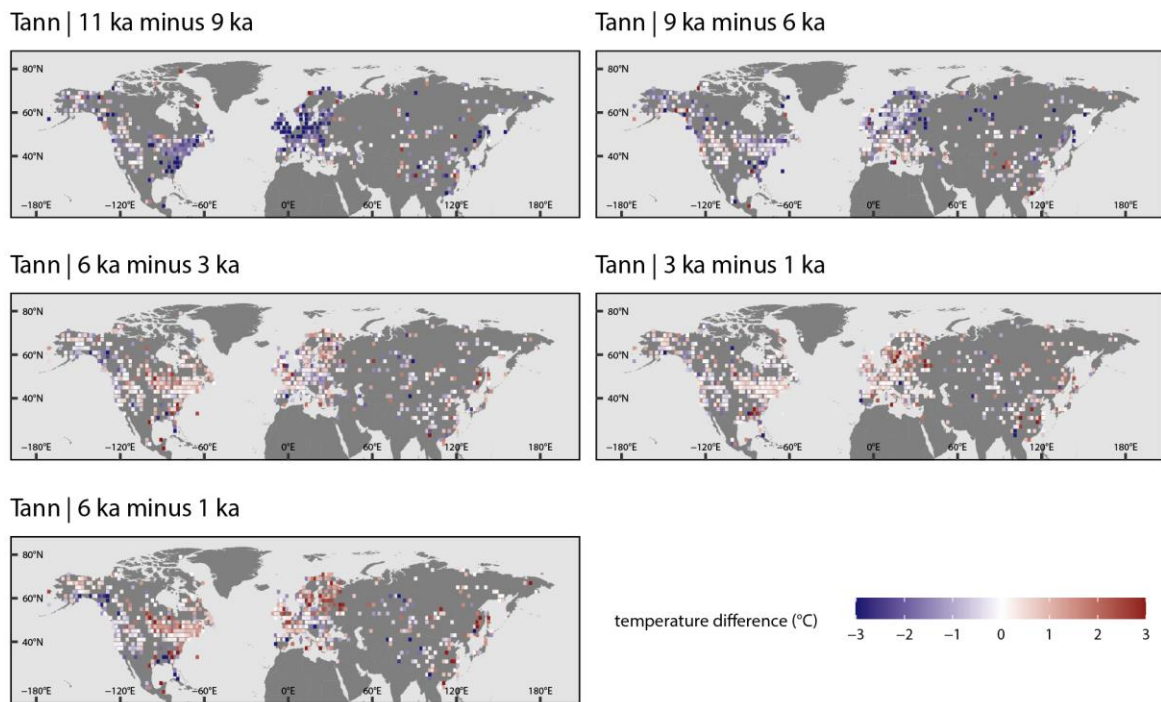
366

367

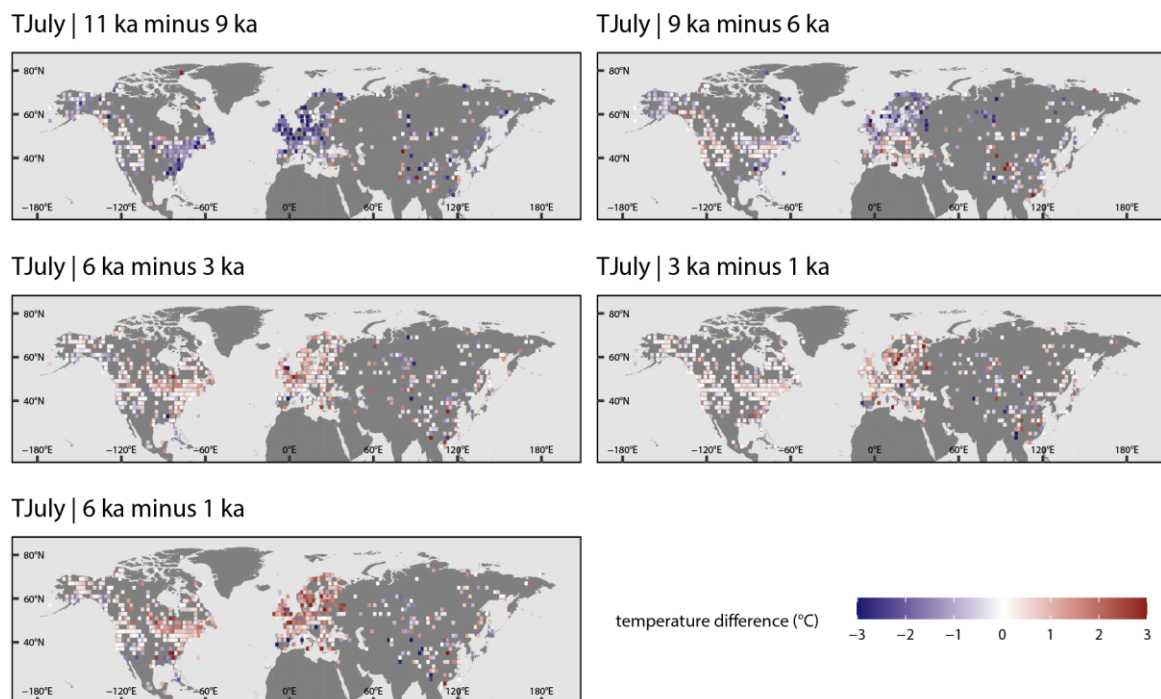
Figure 3. Hemispheric, (sub-)continental, and zonal mean curves for T_{July}, T_{ann}, and %P_{ann} derived from pollen-based reconstruction with WA-PLS. Curves from zonal bands that contain fewer than three grid cells were excluded. The shading corresponds to the latitude-weighted standard error of the

368 latitude-weighted mean. Labels in corresponding colors indicate the number of grid boxes that
369 contributed to each latitudinal curve.

370

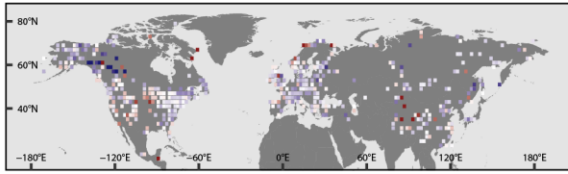


371

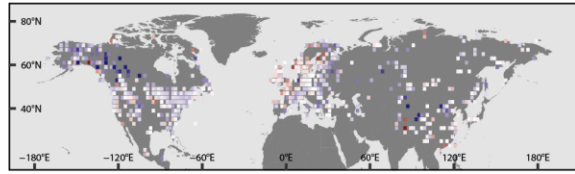


372

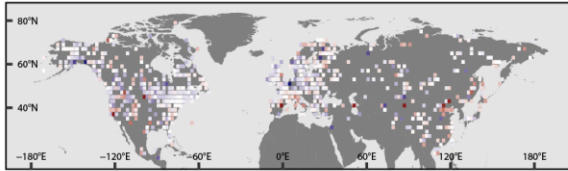
%Pann | 11 ka minus 9 ka



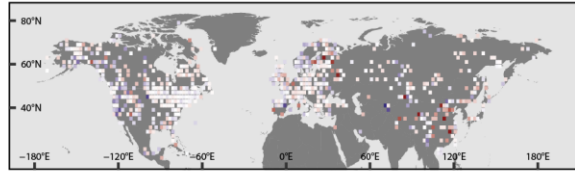
%Pann | 9 ka minus 6 ka



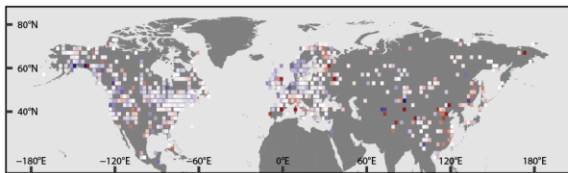
%Pann | 6 ka minus 3 ka



%Pann | 3 ka minus 1 ka

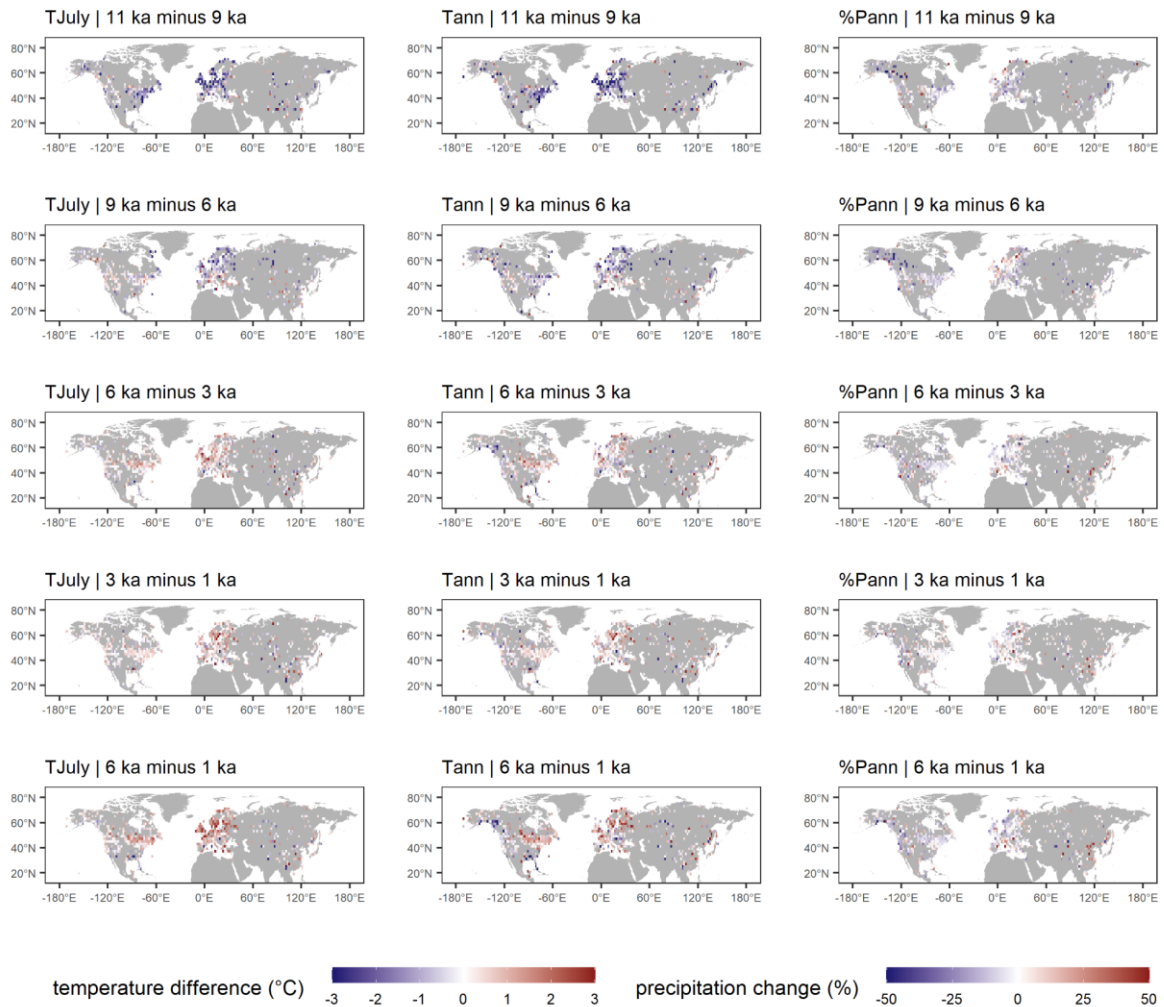


%Pann | 6 ka minus 1 ka



373

374 Hemispheric, continental, and latitudinal mean curves for T_{July} , T_{ann} , and P_{ann} . Curves from latitudinal
375 bands that contain less than three grid cells were excluded.



376

377

378

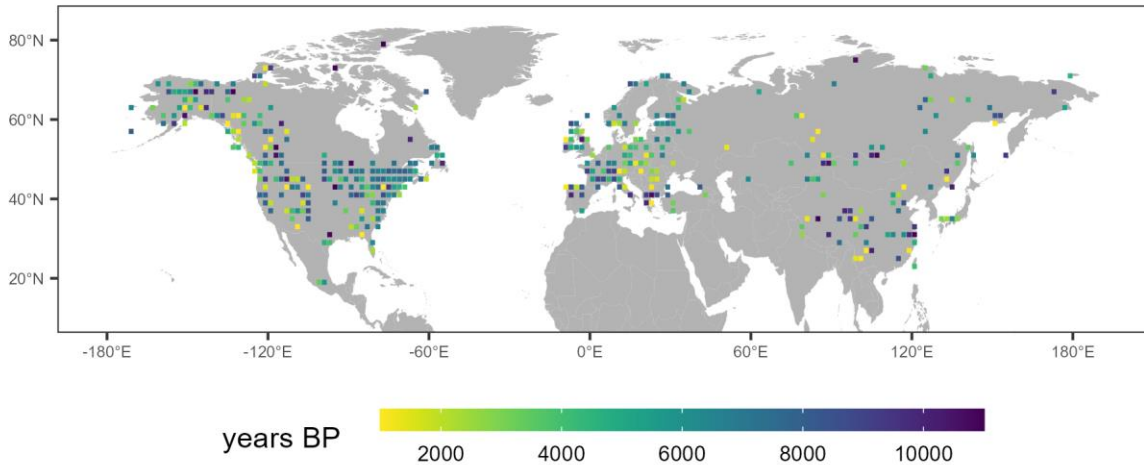
379

380

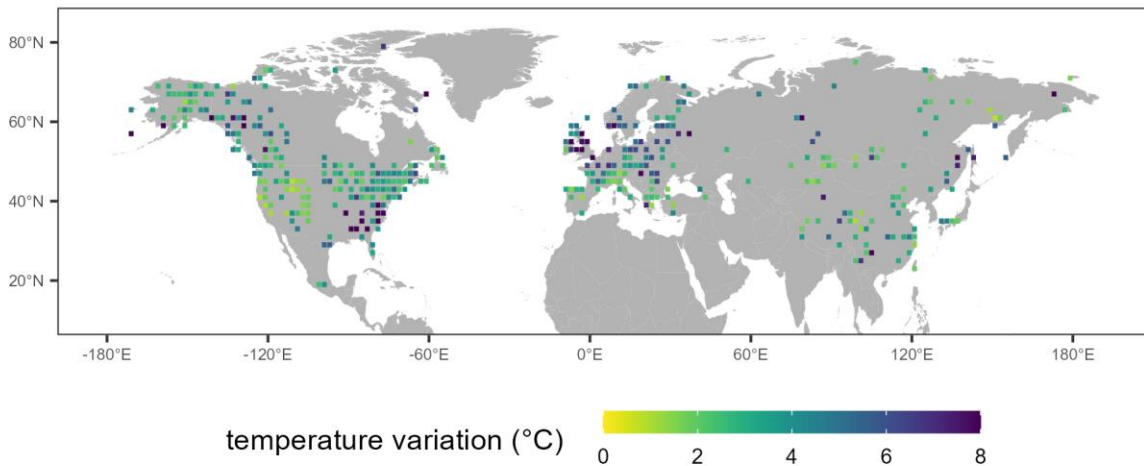
381

Figure 43. Difference maps of T_{July} , T_{ann} (°C), and P_{ann} (as % of the value of the younger time-slice) between selected time-slices. Color code for values outside the range were restricted to range maxima. [A list with the entire value range and the proportions of values that fall within the restricted range are presented in Appendix Table 1.](#) Maps are gridded values averaging the values of records from within the 2°x2° grid-cell.

LegacyClimate 1.0 Dataset | Holocene temperature maximum

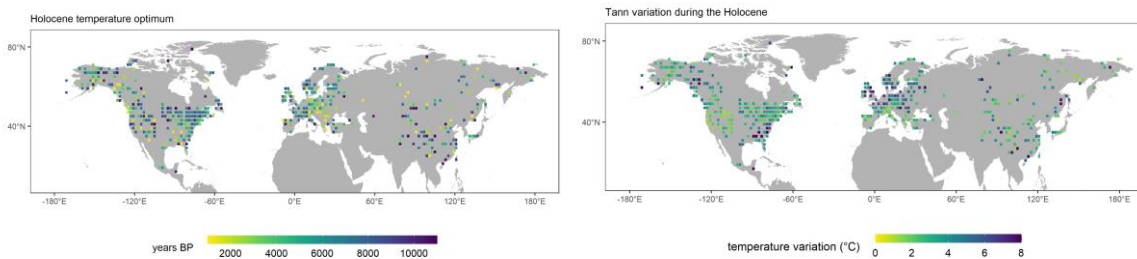


LegacyClimate 1.0 Dataset | Temperature variation during the Holocene



382

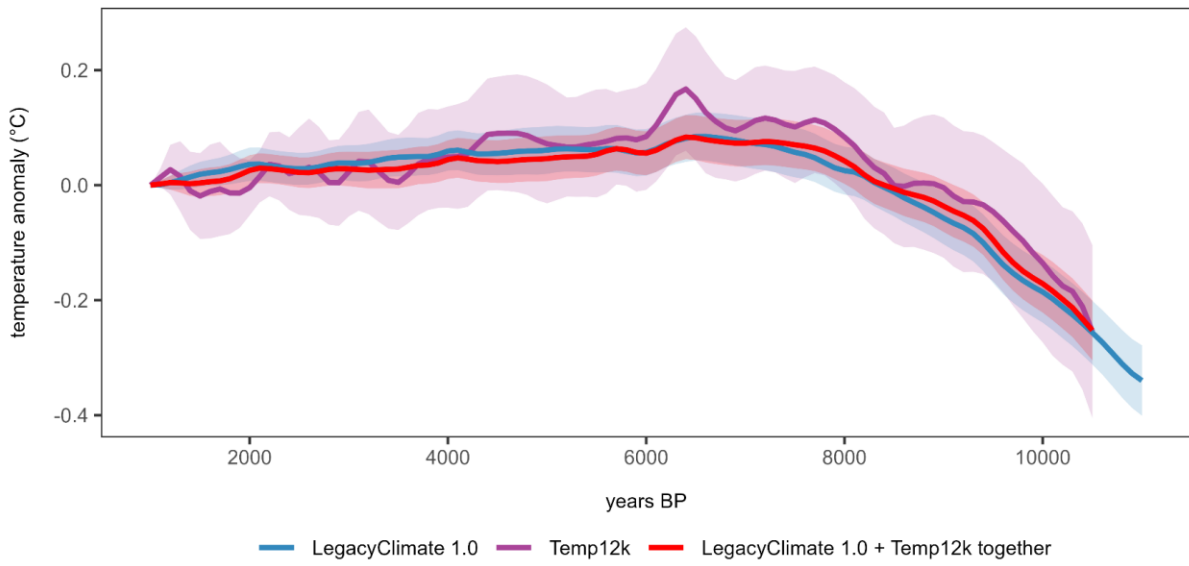
383



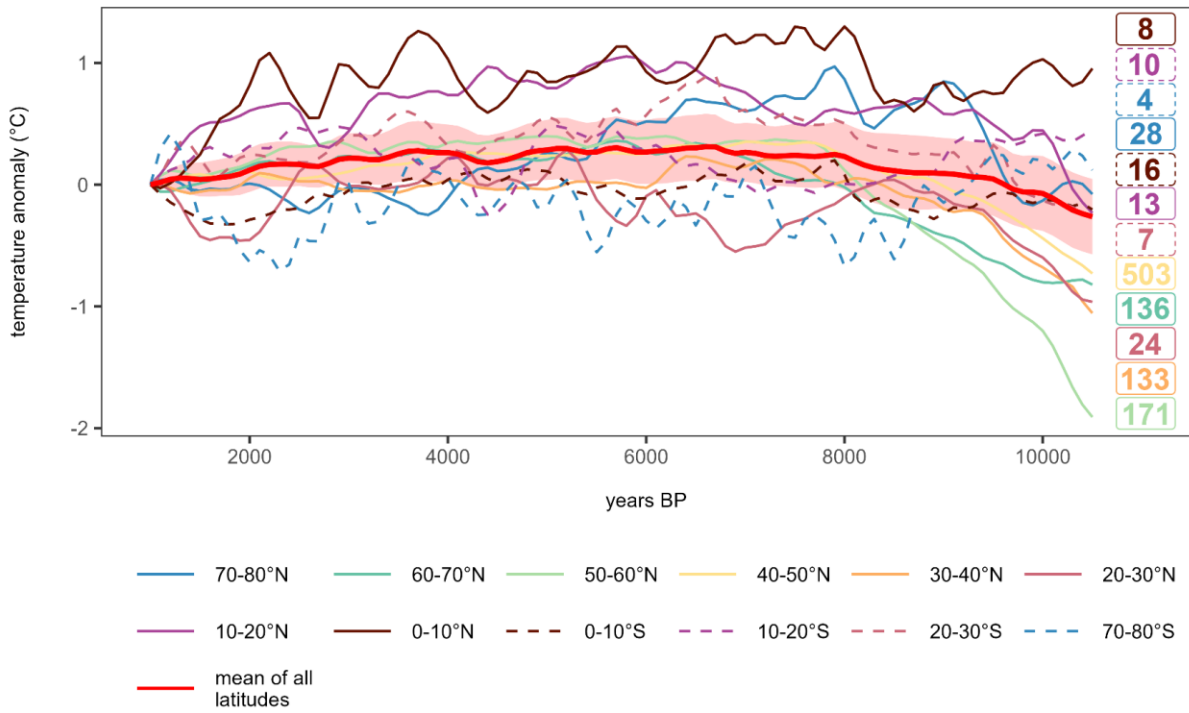
384

385 **Figure 54.** Maps indicating the timing of the T_{ann} **maximum (top optimum (left))** and **the range of T_{ann}**
 386 **variation during the Holocene (11-1 ka, bottom right).** Each $2^\circ \times 2^\circ$ grid cell contains the averaged
 387 values of all records located within one grid cell. For each grid cell, the T_{ann} variation was determined as
 388 the range between minimum and maximum T_{ann} anomalies. **The For T_{ann} Holocene temperature**
 389 **maximum optimum** is the timing of the anomaly maximum. Color code for values outside the range were
 390 restricted to range maxima.

LegacyClimate 1.0 + Temp12k | Tann Northern Hemisphere

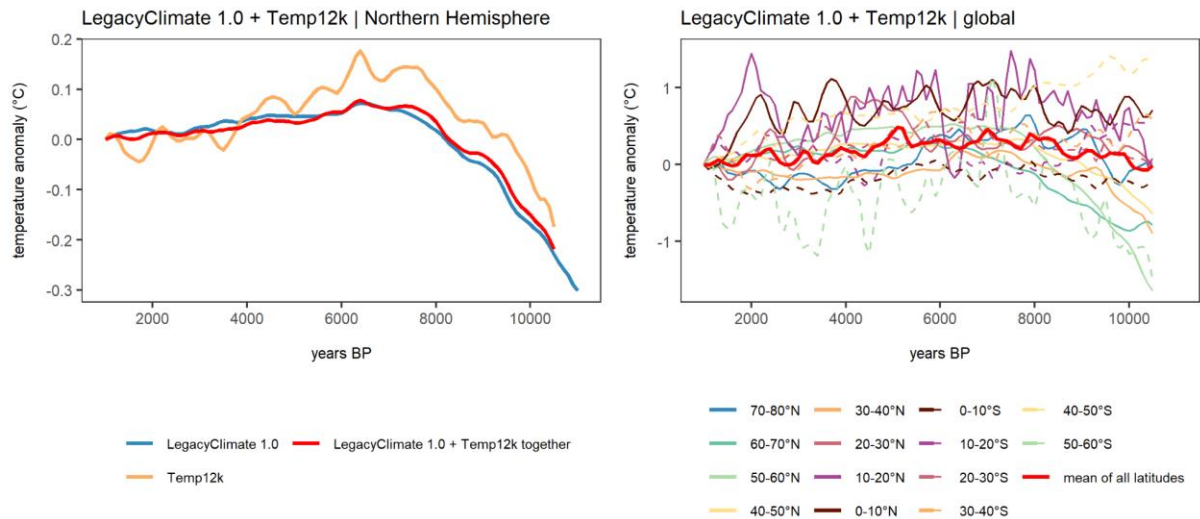


LegacyClimate 1.0 + Temp12k | Tann global



391

392



393
 394 **Figure 65. Mean curves for temperature.** (top)Left: Northern Hemisphere weighted means with
 395 shaded weighted standard error only (no curves for latitudes): LegacyClimate 1.0 LegacyClimate4.0
 396 (n=957; blue), Temp12k dataset (n=272 orange, see methods for record filter; purple.), LegacyClimate
 397 1. LegacyClimate4.0 + Temp12k mean (n=1098; red); (bottom) LegacyClimate 1.0 right:
 398 LegacyClimate4.0 + Temp12k global mean with latitudinal means. Labels in corresponding colors
 399 indicate the number of grid boxes that contributed to each latitudinal curve.

400

401 4 Discussion

402 4.1 Spatial temperature pattern (in light of the global Holocene temperature curve)

403 The general pattern of the LegacyClimate 1.0 LegacyClimate4.0 mean annual temperature curve of the
 404 Northern Hemisphere extratropics agrees with those of previous investigations (Marcott et al., 2013;
 405 Kaufman et al., 2020b; Kaufman and Broadman, 2023) including a cold Early Holocene, a
 406 temperature maximum during the Early to Mid-Holocene, and a slight cooling towards the
 407 present-day (Fig. 2; Appendix Fig. 8). Orbital forcings are assumed to have an important influence on
 408 the trends in the global mean temperatures, which led to feedback mechanisms like decreased polar
 409 sea ice or shifted vegetation ranges and thus to increased temperatures during the Mid-Holocene
 410 (Kaufman and Broadman, 2023). Subsequently, changes in solar irradiance, an increasing albedo due
 411 to land-cover changes and increasing volcanic activity probably contributed to a global cooling during
 412 the Late Holocene (Kaufman and Broadman, 2023). Both our LegacyClimate 1.0 ~~curve~~ and the
 413 Temp12k mean temperature curves increase from the Early Holocene to the Mid-Holocene by about
 414 0.4°C ~~from the early Holocene to the mid-Holocene~~ when the same stacking approach ~~as has been~~
 415 ~~applied to the LegacyClimate 1.0 dataset~~ is applied. However, the LegacyClimate 1.0 LegacyClimate4.0
 416 stack shows only a minimal temperature decline between the early Mid-Holocene maximum and the
 417 Late ~~late~~-Holocene minimum of ~~~0.08°C~~ ~~07K~~ compared to ~~~0.17°C~~ ~~18K~~ in the Temp12k stack. We
 418 suggest two probable reasons for this finding: 1) a more complete spatial and temporal

419 representativeness of the dataset, and 2) a unique methodology to reconstruct a small set of climate
420 variables from pollen data.

421 First, our mean annual temperature curve includes about four times ~~as many the number of~~ records
422 ~~as compared with~~ the Temp12k dataset (~~957994~~ records in the LegacyClimate 1.0 dataset vs. ~~272249~~
423 records in the Temp12k dataset, Kaufman et al. 2020b; ~~)(~~Fig. 14a). In particular, Asia is represented by
424 ~~substantially~~ more records in the combined dataset. Our temperature reconstruction from Asia shows
425 an average trend that differs from the overall Northern Hemisphere trend as it has no ~~pronounced~~
426 ~~Holocene temperature maximum (Appendix Fig. 8; Appendix Table 6).~~~~Holocene optimum.~~ This is
427 particularly true for Asian T_{ann} records south of 50°N and T_{July} records south of 60°N. This feature has
428 not been recognized so far, likely because Asian temperature reconstructions are mostly lacking in
429 previous compilations (e.g., Marcott et al., 2013; Marsicek et al., 2018; Routson et al., 2019; Kaufman
430 et al., 2020b). Even if the ~~Mid- mid-~~ ~~Late-late~~ Holocene cooling trend observed in Asia north of 60°N
431 ~~(Fig. 2)~~ agrees with the proposed Neoglacial (sub-)arctic-~~wide~~ Holocene cooling, the amount of cooling
432 of <0.5°C is low compared to the cooling observed in other regions (e.g., in Europe where an average
433 cooling of ~1.5°C has been reconstructed; McKay et al., 2018; ~~Fig. 2~~). As with the differences between
434 Eastern and Western Eurasia, we find a difference between Eastern and Western North America. In
435 particular, we can identify a circum-North Atlantic pattern with a strong ~~Earlyearly~~ Holocene increase,
436 ~~and~~ a pronounced ~~Midmid-~~ Holocene ~~maximumoptimum~~ and strong temperature range, and a circum-
437 North Pacific pattern with an overall weak change. This is likely related to the impact of the decaying
438 Laurentide ice-sheet on the North Atlantic ~~whichthat~~ was probably a stronger driver of ~~Early early-~~ ~~id-~~
439 ~~-mid-~~ Holocene temperature change than insolation (Renssen et al., 2009; Renssen et al., 2012; Zhang
440 et al., 2016).

441 Even if this study shows a less pronounced Holocene temperature ~~maximumoptimum~~, the problem
442 remains that this does not align with the overall Holocene increase in the mean global (and Northern
443 Hemisphere) temperature revealed by Earth System Models. Our study points to a strong regionalization
444 of Holocene temperature trends and range of variation in the Northern Hemisphere extratropics, ~~which~~
445 ~~was also reported in recent studies (e.g. Kaufman et al., 2020b; Osman et al., 2021; Cartapanis et al.,~~
446 ~~2022).~~ This somehow contradicts the 'Holocene conundrum' concept which tackled Holocene
447 temperature change mainly ~~byfrom~~ analyzing the ~~globalGlobal~~ mean and understanding the differences
448 between proxy-based and simulated reconstructions. ~~However, the conundrum debate has since~~
449 ~~progressed and recent studies hint at discrepancies in data-model comparisons due to spatiotemporal~~
450 ~~dynamics related to heterogeneous responses to climate forcing and feedbacks (e.g., the timing of a~~
451 ~~Holocene thermal maximum between reconstructions from continental and from marine proxy records;~~
452 ~~Cartapanis et al., 2022).~~ Our finding is in line with recent modeling approaches, which also yield strong
453 regional differences in temperature developments (Bader et al., 2020) allowing for a regional comparison.
454 Recent ~~paleopalaeo-~~data assimilation approaches based on marine temperature reconstructions reveal
455 peculiarities of spatial averaging as one reason for the model-data mismatch (Osman et al., 2021). The
456 error is most pronounced where the number of included records is small. This stresses the importance
457 of ~~a-~~good spatial coverage of the records used for the assessment of the mean temperature trend.

458 Including terrestrial reconstructions is crucial. Compared with previous syntheses of terrestrial records,
459 our compilation is ~~notable for its particularly characterized by a~~ higher record density in Asia, a region
460 for which Earth System Models show diverging past climate changes, highly sensitive to boundary
461 conditions and forcing (Bakker et al. 2020; Brierley et al., 2020; Lohmann et al. 2021). Therefore, our
462 reconstruction makes a decisive contribution to locating and clarifying the model-data mismatch in the
463 Northern Hemisphere extratropics. From a proxy perspective, future targets of synthesis studies should
464 ~~focus be~~ on the Southern Hemisphere and poorly covered areas in ~~Central~~ Asia and Siberia.

465 Second, standardized methodologies may have contributed to the observed differences between ~~the~~
466 ~~LegacyClimate 1~~ LegacyClimate4.0 mean T_{ann} curve and the Temp12k curve. Our T_{ann} reconstruction
467 only includes records of mean annual temperature while the Temp12k product mixes reconstructions of
468 seasonal temperature (mostly T_{July}) if T_{ann} is not available from a site. This assumption of equivalence
469 between annual and summer temperature at any given site can impact the trend and amplitude of the
470 stacks. ~~A~~ seasonal bias in the reconstructions may originate from a real, larger Holocene range of
471 summer temperature variations (Bova et al., 2021) or is an ~~artefact~~ artifact introduced by having a larger
472 T_{July} range covered by the calibration datasets compared with T_{ann} which is, however, not the case in
473 our calibration sets.

474 Our pollen-based reconstructions are all performed with WA-PLS, which is known to produce smaller
475 climate amplitudes than MAT (a likewise commonly used method) because it is less sensitive to extreme
476 climate values in the modern pollen dataset (Birks and Simpson 2013; Cao et al., 2017; Nolan et al.
477 2019). Furthermore, by using a standard area size for our modern pollen datasets, we may have
478 stabilized the regional reconstructions, that is, equalized the amplitude as the source areas represent
479 rather similar biogeographical and climate ranges. Finally, our reconstructions include only records that
480 cover the entire Holocene period (11-1 ka) and not just parts of it. Hence, all time-slices have a similar
481 spatial coverage and the temporal pattern is not biased by regions where archives are only available in
482 certain periods (e.g., the ~~Late late~~ Holocene peatland establishment).

483 As with all applications of taxa-based transfer functions to fossil records, we assume that both modern
484 and past taxa assemblages (in our case, vegetation) are in equilibrium with climate, and that the
485 relationships inferred from modern data do not change throughout the Holocene (Birks et al., 2010;
486 Chevalier et al., 2020) and that the modern pollen assemblages are not heavily biased by human impact.
487 Differences in global boundary conditions during the ~~Early early-to id-mid~~ Holocene (e.g., lower
488 atmospheric CO_2 concentration, different seasonal insolation) however, may have modified these
489 relationships, which could have also dampened the reconstructed amplitudes. ~~Also, vegetation~~
490 ~~response to climate change may be involve lags (see the ongoing discussion about the so-called 'forest~~
491 ~~conundrum', i.e., the observation that observed forest maximum lags the simulated temperature~~
492 ~~maximum; Dallmeyer et al., 2022) and depends on the initial conditions such as the distribution of refugia~~
493 ~~during the Last Glacial (Herzschuh et al., 2016; 2020). Furthermore, there are areas, especially the~~
494 ~~densely settled regions in Europe and Southeastern Asia, that are affected by human activities~~
495 ~~throughout the Holocene due to intense animal husbandry, as inferred from the abundance of~~
496 ~~Plantaginaceae and Rumex as indicators of grazing (Herzschuh et al., 2022a), or due to industrialization~~

497 since the second half of the 19th century. This probably led to extinction events, especially for
498 disturbance-dependent taxa and contributed to gaps within the potential bioclimatic space of taxa that
499 form natural communities (Zanon et al., 2018). The absolute effect of these biases is hard to quantify
500 (but see Cleator et al., 2020), and many comparative, multi-proxy Holocene studies have shown that
501 pollen-based reconstructions are as reliable as any other proxy (Kaufmann et al., 2020a; Dugerdil et al.,
502 2021). In contrast, one advantage of single proxy studies is that any biases will affect all the records
503 similarly. As such, even if the actual amplitude of our regional and global stacks might be dampened,
504 the trends and spatial patterns shared by the data are likely to remain correct.

505

506 **4.2 Spatio-temporal precipitation pattern**

507 Our analyses of the Holocene spatio-temporal precipitation pattern fill a research gap, as syntheses of
508 proxy-based precipitation change on aat the hemispheric scale during the Holocene are still lacking.
509 Regional syntheses are available for Europe (Mauri et al., 2014 and 2015), North America (Ladd et al.,
510 2015; Routson et al., 2021), and Eastern Asia (Herzschuh et al., 2019). Interestingly, we observed a
511 similar pattern for Northern Hemisphere-wide averaged Holocene trends of P_{ann} and T_{ann} , but differences
512 among corresponding P_{ann} and T_{ann} curves at (sub-)continental and latitudinal scales, e.g., in Asia, where
513 the P_{ann} means are overall higher than the Northern Hemispheric means while the T_{ann} means are overall
514 lower since ~ 9 ka (Appendix Fig. 8), or for the 30-40°N zonal band, where T_{ann} shows an Early to Mid-
515 Holocene warming while no trend in the P_{ann} means could be found for this time period (Appendix Fig.
516 3).

517 This regional heterogeneity with respect to the precipitation trend (i.e., significantly different trends for
518 the Northern Hemisphere except for some regions in Asia, Appendix Table 4, Appendix Fig. 8) is also
519 seen in recent Earth System Model simulations for the last 8000 years (Mauri et al., 2014; Dallmeyer et
520 al., 2021). Although the simulated pattern does not exactly match our reconstructions, they share many
521 similar structures such as higha-pronounced-decrease-of precipitation in East Asia since the Early and
522 Midmid-Holocene in East Asia (Fig. 4). For this region, our reconstruction shows the strongest Mid-
523 mid-to Late-late Holocene precipitation decline worldwide, reflecting the weakening of the East Asian
524 Summer Monsoon (EASM) in response to the decrease in summer insolation. This trend in moisture
525 has been confirmed by earlier qualitative and quantitative proxy syntheses and modeling studies (Wang
526 et al., 2010; Zheng et al., 2013; Liu et al., 2014a; Herzschuh et al., 2019).

527 In contrast, many Centralcentral Asian sites show low Early-Holocene indicate an increase in
528 precipitation levels (Fig. 4) from the early to mid-Holocene. This anti-phase relationship in EASM to
529 Centralcentral Asian moisture change is in line with earlier studies (Jin et al., 2012; Chen et al., 2019;
530 Herzschuh et al., 2019; Zhang et al., 2021). The causal mechanisms are still debated. Among other
531 reasons, precipitation-evaporation effects (Herzschuh et al., 2004; Zhang et al., 2011; Kubota et al.,
532 2015), transcending air mass related to the Rodwell-Hoskins response to monsoonal heating
533 (Herzschuh et al., 2004; Wang et al., 2017), effects from winter precipitation (Li et al., 2020), and

534 translocation of the westerly jetstream (Herzschuh et al., 2019) may contribute to the anti-phased
535 precipitation change.

536 Arctic warming mechanistically should be linked with wetting in the Arctic due to high hydrological
537 sensitivities (Trenberth, 2011). Such a pattern is, for example, obvious for ~~Early early-to id--mid~~
538 Holocene climate change in most records from Alaska. Interestingly, several records from the northern
539 Arctic coastal region in Russia, northern Norway, and Canada show a wet ~~Earlyearly~~ Holocene, which
540 is also observed in simulations (Dallmeyer et al., 2021).

541 Contrasting the trend in the East Asian monsoon region (~~Fig. 2; Appendix Fig. 7~~), annual precipitation
542 increases in mid-latitude Europe during the Holocene according to our reconstructions (~~Fig. 2; Appendix~~
543 ~~Fig. 6~~). Routson et al. (2019) propose a circum-hemispheric mid-latitudinal rise of moisture levels over
544 the Holocene based on a semi-quantitative dataset that is strongly concentrated around the circum-
545 Atlantic region. They relate the decreased net precipitation to the weakened ~~Early early~~-Holocene
546 latitudinal temperature gradient. Due to polar amplification, the arctic regions experienced a stronger
547 warming in the climate compared to the equatorial region, which is also ~~supported~~~~confirmed~~ by our
548 dataset. However, we also see in our reconstructions that this view is too general, but it may explain the
549 precipitation response in Europe as the weakening of the latitudinal temperature gradient is particularly
550 pronounced in Europe in our reconstructions. This change in temperature pattern is probably a result of
551 a dampening in the cyclonic activity along the weaker westerly jet (Chang et al., 2002; Routson et al.,
552 2019; Xu et al., 2020), bearing less precipitation during the ~~Earlyearly~~ Holocene compared to modern
553 conditions. With the strengthening of the latitudinal temperature gradient towards the ~~Latelate~~ Holocene,
554 cyclonic activity enhances, leading to an increase of precipitation over the Holocene.

555 According to our reconstructions, the precipitation trend in Eastern and Western North America strongly
556 differs ($p < 0.01$; ~~Appendix Table 5; Fig. 32~~). While in the ~~Easterneastern~~ part the mean precipitation
557 level is relatively stable in all latitudinal bands, ~~except the 50-60°N zonal band~~, over the Holocene
558 (~~Appendix Fig. 5~~), precipitation strongly increases on average in the ~~Westernwestern~~ part (~~Appendix~~
559 ~~Fig. 4~~), driven by a precipitation rise in the mid-latitudes (40-70°N). In the polar regions and south of
560 40°N, precipitation declines from the ~~Midmid~~-Holocene (Fig. 4; ~~Appendix Fig. 43~~). The latter may be
561 related to a decrease in the North American monsoon intensity, in line with the orbital monsoon
562 hypothesis (Kutzbach, 1981; Harrison et al., 2003). In the polar region, modeling studies report
563 northward shifted storm tracks coinciding with a northward replaced upper tropospheric jetstream in the
564 ~~Midmid~~-Holocene compared to the ~~Latelate~~ Holocene, promoting precipitation in the arctic region and
565 decreasing precipitation at mid-latitudes (Zhou et al., 2020; Dallmeyer et al., 2021). With the southward
566 shift of the polar jet during the Holocene, precipitation decreased in the high northern latitudes in North
567 America and increased further south (Liu et al., 2014b).

568 The rise in moisture levels across the North American continental interior over the course of the
569 Holocene has been proposed before (Grimm et al., 2001; Zhou et al., 2020; Dallmeyer et al., 2021) but
570 has not yet been quantified with continental-wide proxy-data. The main drivers of this trend are still being
571 debated: besides shifts in the westerly wind circulation (Seager et al., 2014), weakening subsidence

572 caused by teleconnection with the weakening ~~Northern Hemispheric~~~~northern hemispheric~~ monsoon
573 systems (Harrison et al., 2003; Dallmeyer et al., 2021), ~~reorganization~~~~re-organization~~ of the atmospheric
574 circulation around the Bermuda high (Grimm et al., 2001), and changes in the sea-surface temperature
575 pattern (Shin et al., 2006) may contribute to an increase in precipitation over the Holocene.

576 Reconstructing temperature and precipitation from a single dataset implies that they are both important
577 in defining the presence and/or abundance of specific pollen taxa (Salonen et al., 2019). This hypothesis
578 cannot be tested but to some extent has been assessed by several analyses (Juggins, 2013). The WA-
579 PLS ~~reconstruction~~ was also applied with tailored modern calibration sets (i.e., selecting samples so
580 that the correlation between temperature and precipitation in the calibration dataset is reduced). The
581 finding that the reconstructions were generally very similar between those using the full and those using
582 the tailored modern datasets can be taken as an indication that co-variation is not a major issue in these
583 reconstructions (Herzschuh et al., 2022a). This conclusion is also supported by the fact that T_{ann} and
584 P_{ann} records that pass the reconstruction significance test when the impact of the other variable is
585 partialled out (Telford and Birks, 2011), are almost evenly distributed over the Northern Hemisphere
586 records (Herzschuh et al., 2022a). This is also confirmed by the visual inspection of the regional
587 reconstructions in Fig. 32, where we cannot detect correlations between variables within latitudinal
588 zones, as would be expected from dependent reconstructions. This suggests that our reconstructions
589 do reflect distinctive trends from the pollen data.

590

591 **5 Conclusions**

592 We investigated Holocene time-series of T_{July} , T_{ann} , and P_{ann} for the Northern Hemisphere extratropics
593 making use of ~~2593~~~~2594~~ pollen-based reconstructions (LegacyClimate 1.0). Compared with previous
594 datasets, we include many more records, particularly from Asia. We present mean curves obtained with
595 the same method for the ~~Northern Hemisphere~~~~hemisphere~~, the (sub-)~~continent~~~~continent~~ (Asia, Europe,
596 Eastern North America, Western North America), and regional zones (i.e., 10° latitudinal bands for
597 (sub-)continents) as well as Northern Hemisphere gridded data for selected time-slices.

598 Our results indicate that Holocene climate change shows unique regional patterns. The concept of a
599 ~~Midmid~~-Holocene temperature ~~maximum~~~~optimum~~ only applies mainly to the mid and high northern
600 latitudes in the circum-North Atlantic region while records from mid-latitude Asia, Western North America,
601 and all subtropical areas do not fit into this concept but mostly show an overall Holocene increase or
602 other ~~patterns~~~~pattern~~. As such, the 'Holocene conundrum' ~~concept~~, originally proposed as a global
603 feature, may instead apply to a restricted region.

604 The precipitation trend is roughly similar ~~to~~~~with~~ the temperature trend at the hemispheric scale, in
605 particular with respect to the strong increase from the ~~Early~~~~early~~ to ~~Midmid~~-Holocene. At the regional
606 scale, the precipitation trends differ from each other and also from the regional temperature trends. The
607 ~~30-40-50°~~ latitudinal band in Asia shows the most pronounced ~~Midmid~~-Holocene precipitation
608 ~~maxima~~~~optima~~ while many regions show increasing Holocene trends including most of Europe and

609 Western North America. We relate these differences to regionally specific circulation mechanisms and
610 their specific relationships with temperature changes.

611 Given a background of strong regional heterogeneity, the calculation of global or hemispheric means
612 might generally lead to misleading concepts but the focus should be on understanding the spatio-
613 temporal patterns requiring spatially dense proxy-datasets for comparison with simulations.

614

615 **6 Data Availability**

616 The compilation of reconstructed T_{July} , T_{ann} , and P_{ann} , is open access and available at PANGAEA
617 (<https://doi.pangaea.de/10.1594/PANGAEA.930512>; in the “Other version” section). The dataset files
618 are stored in machine-readable data format (.CSV), which are already separated into Western North
619 America, Eastern North America, Europe, and Asia for easy access and use.

620

621 **Author contributions.** UH designed the study. The analyses were led by UH and implemented by TB.
622 UH guided the interpretation of the results and collected detailed comments from AD, MC, OP, CL, and
623 RH. All co-authors commented on the initial version of the manuscript.

624

625 **Competing interests.** The authors declare that they have no conflict of interest.

626

627 **Acknowledgements.** We would like to express our gratitude to all the palynologists and geologists who,
628 either directly or indirectly by providing their work to the Neotoma Paleocology Database, contributed
629 pollen data and chronologies to the dataset. The work of data contributors, data stewards, and the
630 Neotoma community is gratefully acknowledged. We also thank Cathy Jenks for language editing.

631

632 **Financial support.** This research has been supported by the European Research Council (ERC Glacial
633 Legacy 772852 to UH) and the PalMod Initiative (01LP1510C to UH). TB, MC, and AD are supported
634 by the German Federal Ministry of Education and Research (BMBF) as a Research for Sustainability
635 initiative (FONA; <https://www.fona.de/en>) through the PalMod Phase II project (grant no. FKZ:
636 01LP1926D and 01LP1920A). CL holds a scholarship from the Chinese Scholarship Council (grant no.
637 201908130165). NR work was supported by the Russian Science Foundation (Grant No. 20-17-00110).

638

639

640

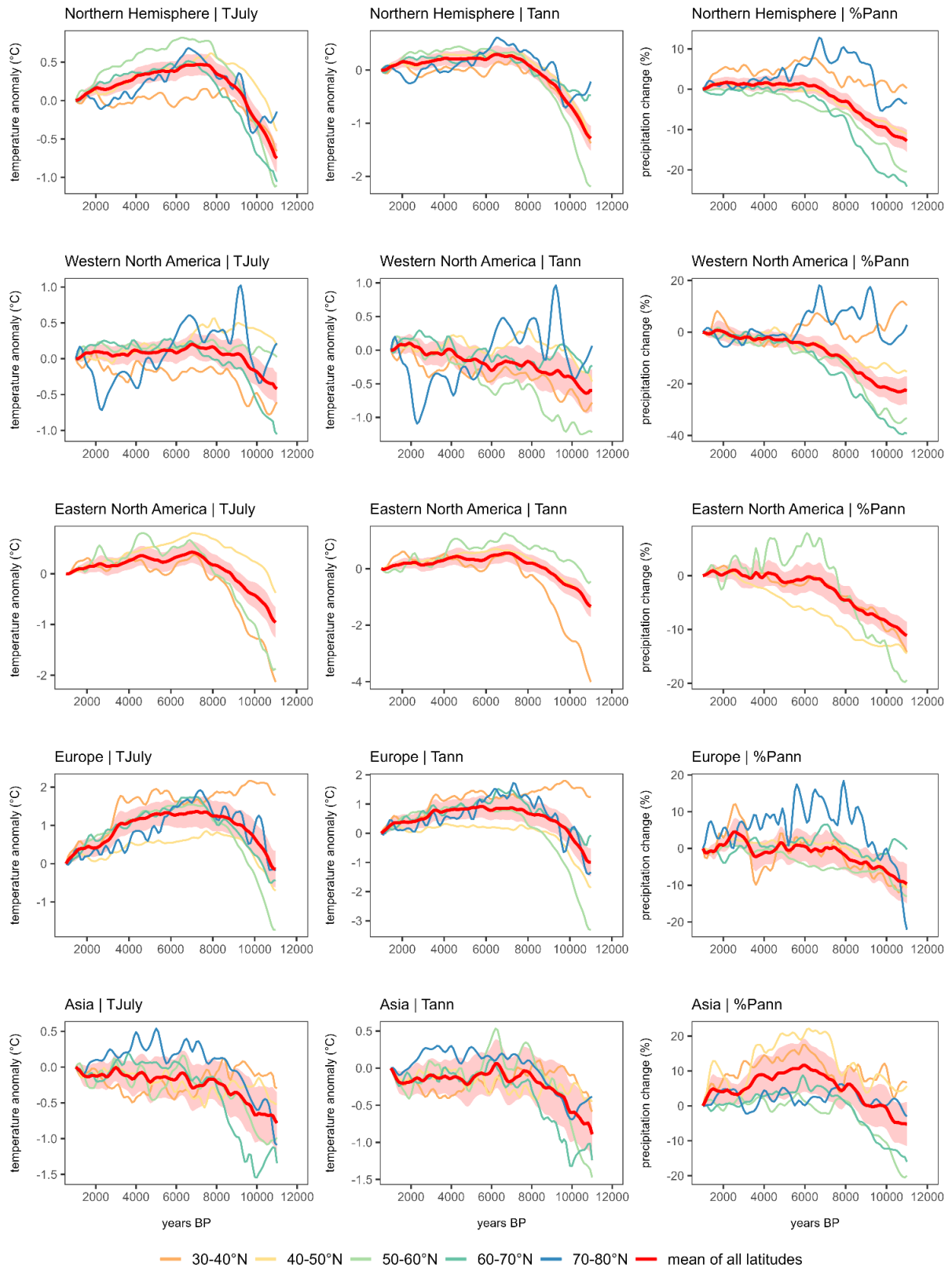
641

642 **Appendix**

643

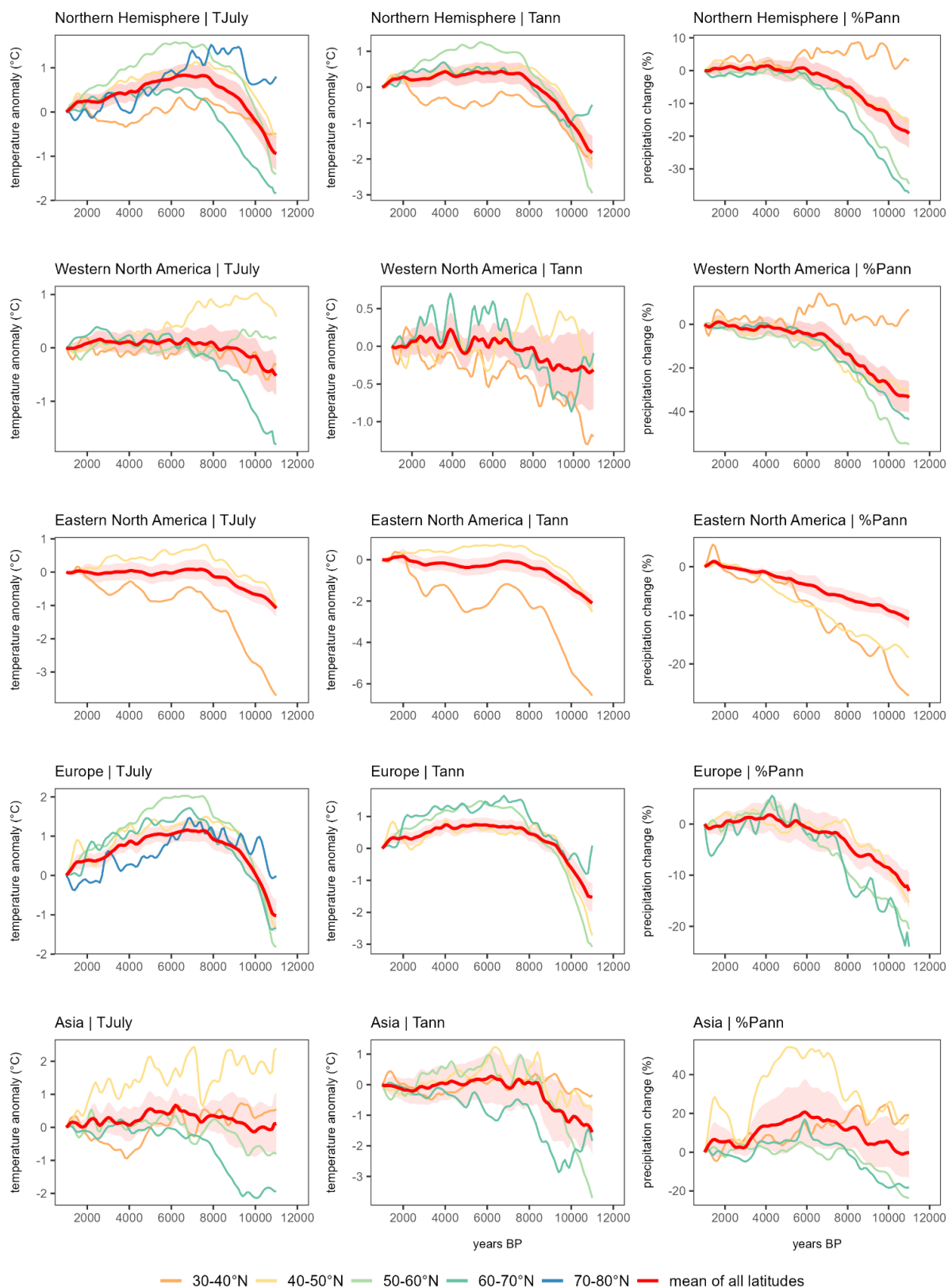
644 **Appendix Table 1.** Range of values in the difference maps (Fig. 4) and proportion of values that fall
645 within a restricted range of -3 to +3 °C for temperature and -50% to 50% for precipitation change.

	<u>T_{July}</u>		<u>T_{ann}</u>		<u>P_{ann}</u>	
	<u>Value range</u>	<u>% within restricted range</u>	<u>Value range</u>	<u>% within restricted range</u>	<u>Value range</u>	<u>% within restricted range</u>
<u>11-9 ka</u>	<u>-12.3°C to +8.2°C</u>	<u>87.8 %</u>	<u>-20.0°C to +6.0°C</u>	<u>79.7 %</u>	<u>-131.7% to +151.3%</u>	<u>96.9 %</u>
<u>9-6 ka</u>	<u>-6.1°C to +16.4°C</u>	<u>95.8 %</u>	<u>-8.9°C to +12.0°C</u>	<u>92.9 %</u>	<u>-81.4% to +103.9%</u>	<u>98.4 %</u>
<u>6-3 ka</u>	<u>-8.2°C to +6.4°C</u>	<u>98.1 %</u>	<u>-8.0°C to +7.9°C</u>	<u>96.5 %</u>	<u>-175.1% to +423.6%</u>	<u>98.8 %</u>
<u>3-1 ka</u>	<u>-10.1°C to +4.6°C</u>	<u>98.2 %</u>	<u>-11.0°C to +10.1°C</u>	<u>97.2 %</u>	<u>-1157.4% to +90.7%</u>	<u>99.0 %</u>
<u>6-1 ka</u>	<u>-9.6°C to +6.5°C</u>	<u>94.9 %</u>	<u>-8.9°C to +9.0°C</u>	<u>93.6 %</u>	<u>-67.6% to +694.3%</u>	<u>98.2 %</u>



646

647 **Appendix Figure 1: Hemispheric, continental, and latitudinal mean curves for T_{July} , T_{ann} , and P_{ann}**
 648 **derived from pollen-based reconstruction with WA-PLS tailored. Latitudinal bands that contain**
 649 **fewer than three grid cells are not shown. The shading corresponds to the latitude-weighted standard**
 650 **error of the latitude-weighted mean.**



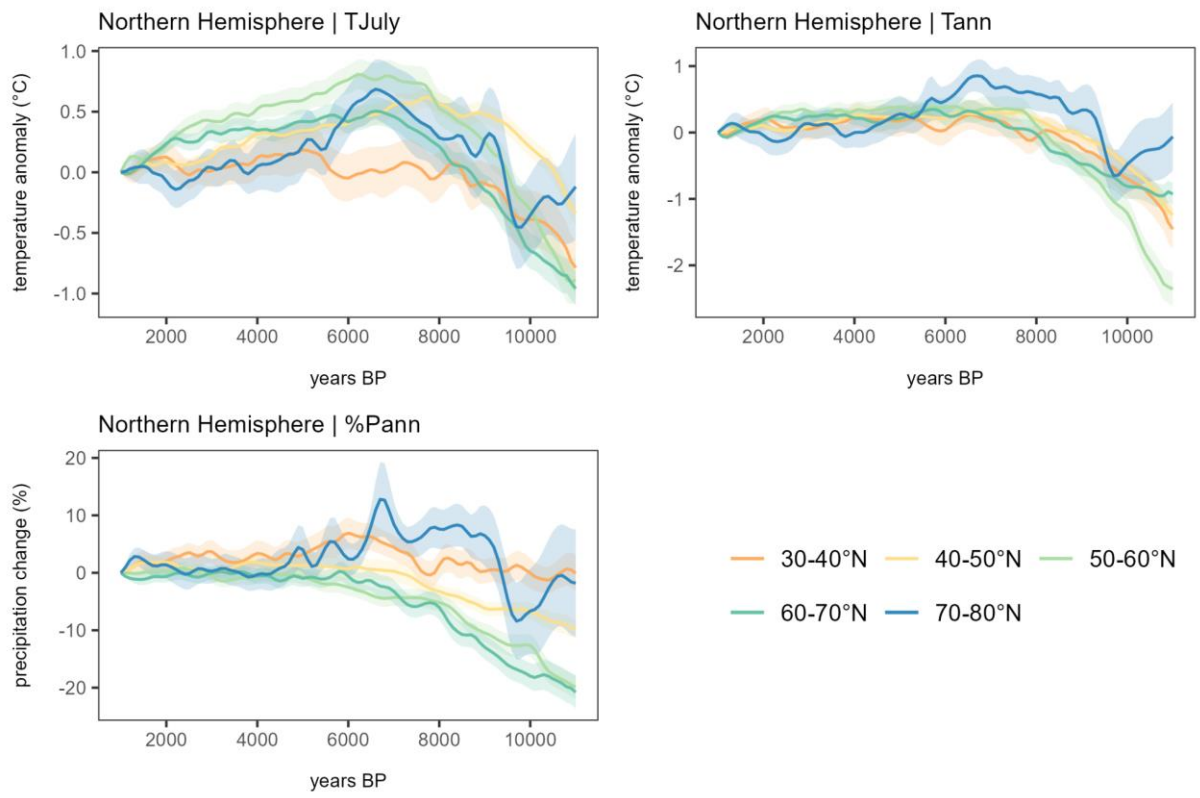
651

652 **Appendix Figure 2: Hemispheric, continental, and latitudinal mean curves for T_{July} , T_{ann} , and P_{ann}**

653 **derived from pollen-based reconstruction with WA-PLS tailored with significant records ($p < 0.2$).**

654 Latitudinal bands that contain fewer than three grid cells are not shown. The shading corresponds to the

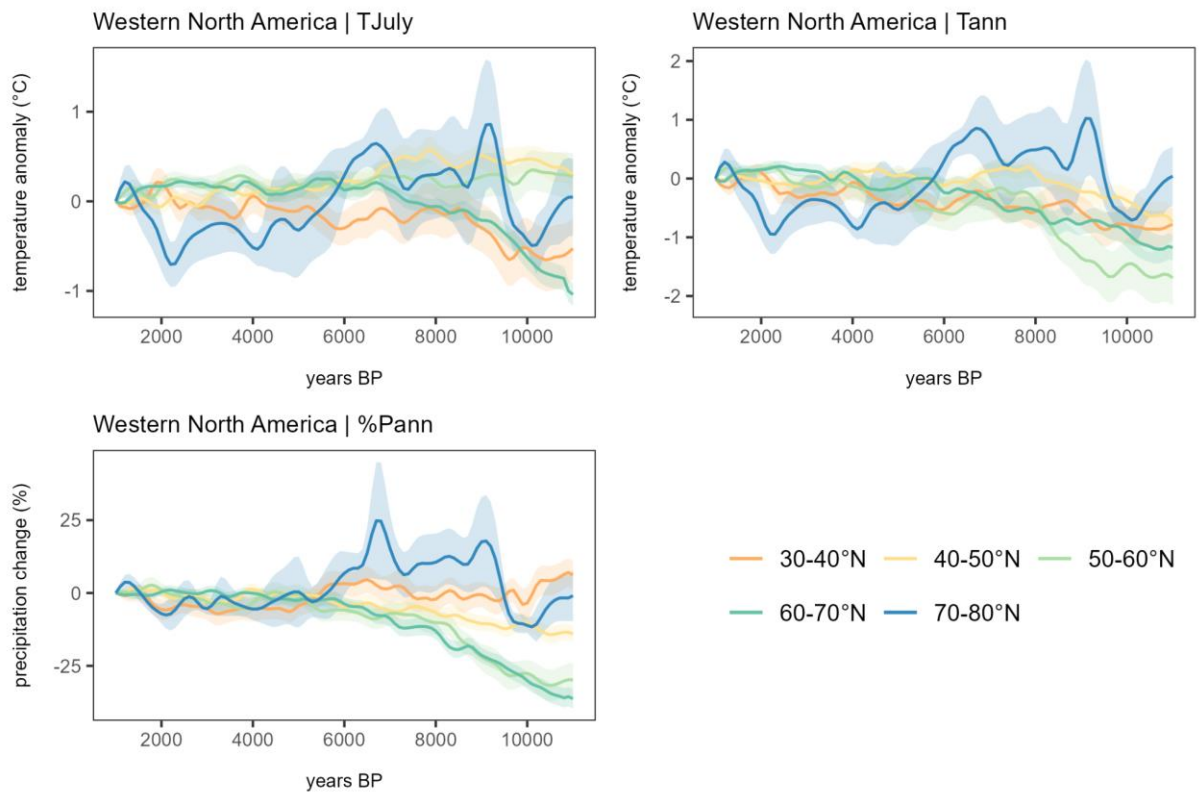
655 latitude-weighted standard error of the latitude-weighted mean.



656

657 **Appendix Figure 3: Northern Hemispheric latitudinal mean curves with shaded standard errors**
 658 **for T_{July}, T_{ann}, and %P_{ann} derived from pollen-based reconstruction with WA-PLS (latitudinal**
 659 **bands that contain fewer than three grid cells are not shown).**

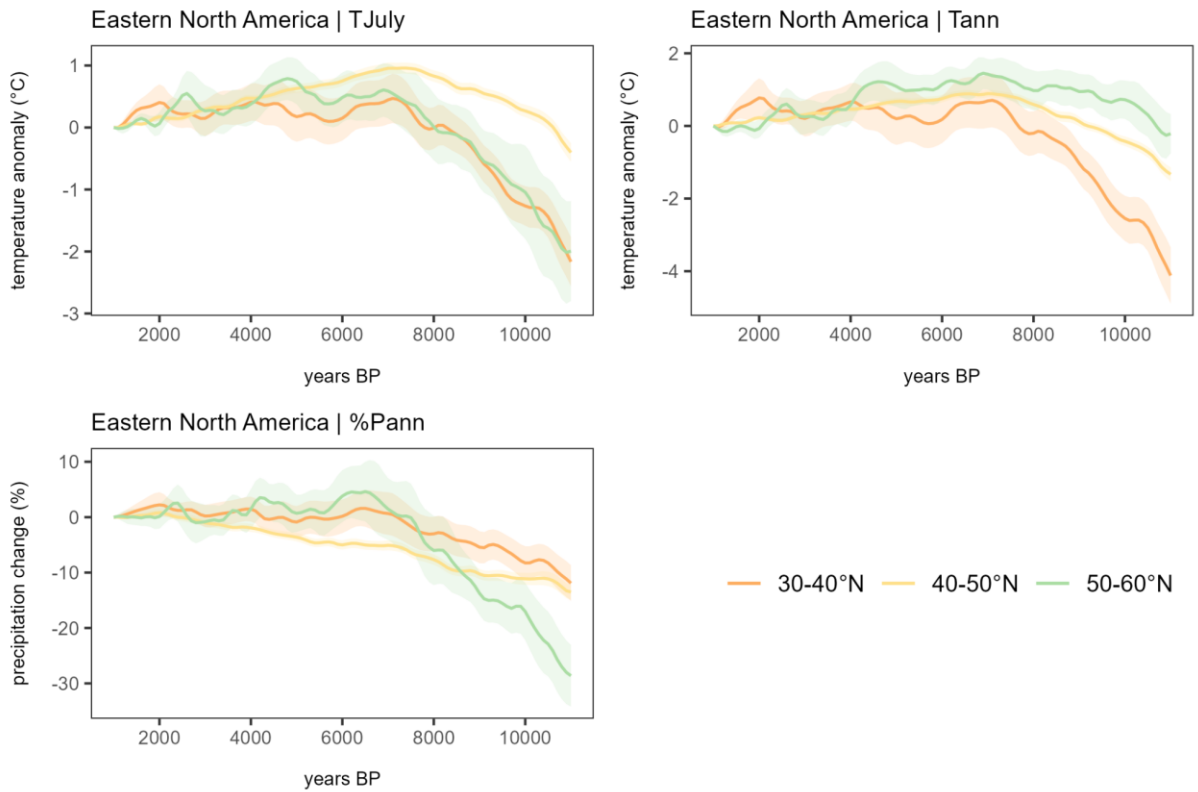
660



661

662 **Appendix Figure 4: Western North American latitudinal mean curves with shaded standard errors**
 663 **for T_{July}, T_{ann}, and %P_{ann} derived from pollen-based reconstruction with WA-PLS (latitudinal**
 664 **bands that contain fewer than three grid cells are not shown).**

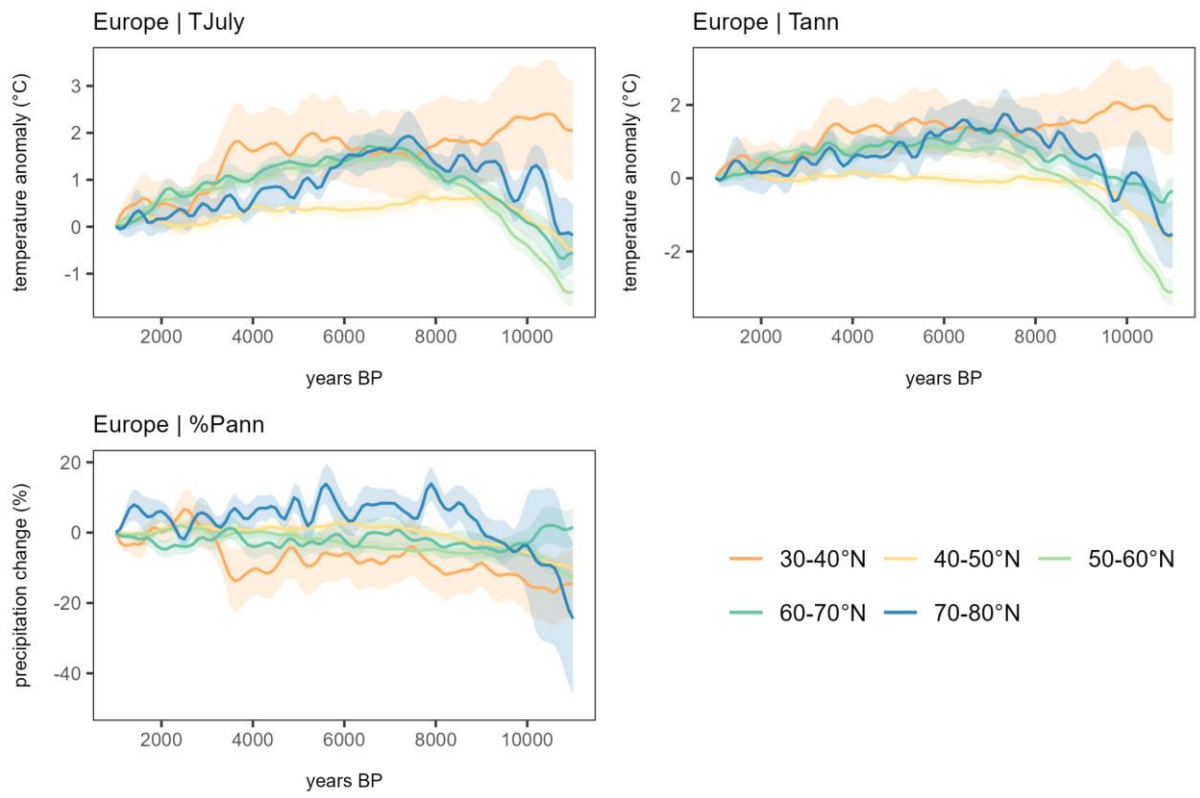
665



666

667 **Appendix Figure 5: Eastern North American latitudinal mean curves with shaded standard errors**
 668 **for T_{July}, T_{ann}, and %P_{ann} derived from pollen-based reconstruction with WA-PLS (latitudinal**
 669 **bands that contain fewer than three grid cells are not shown).**

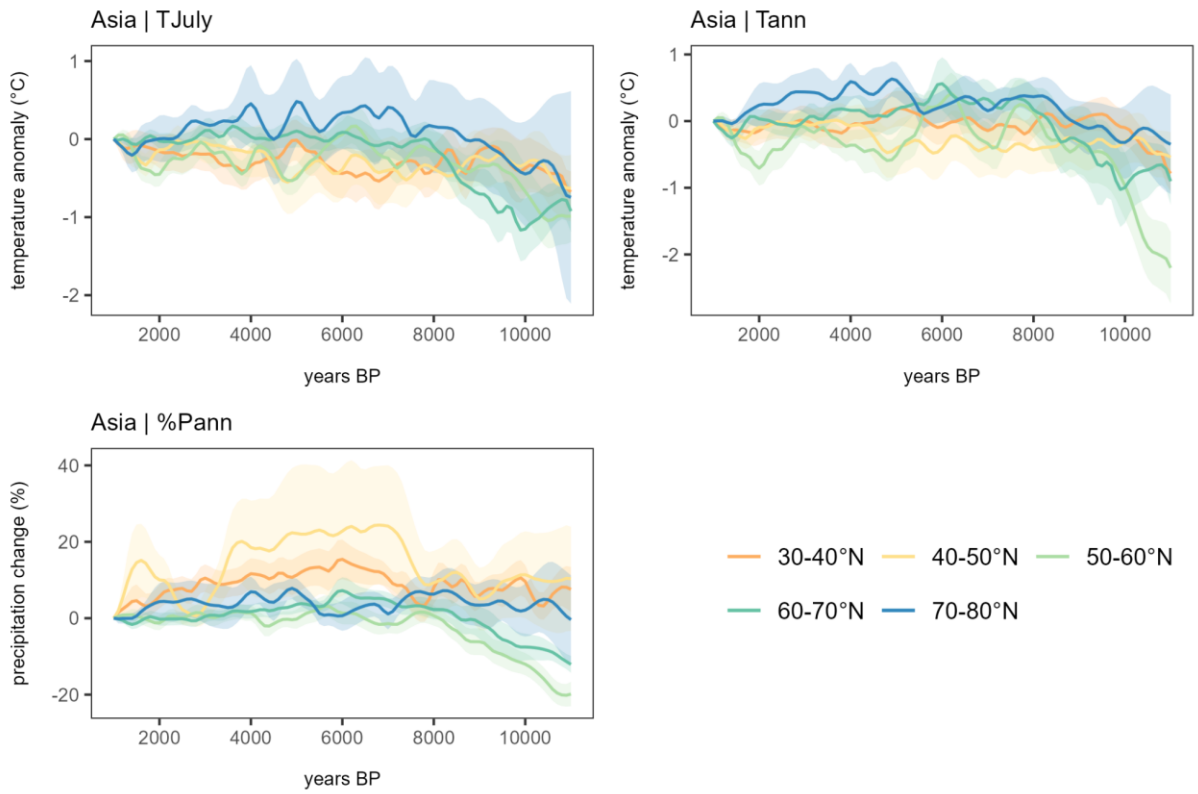
670



671

672 **Appendix Figure 6: European latitudinal mean curves with shaded standard errors for T_{July} , T_{ann} ,**
 673 **and $\%P_{ann}$ derived from pollen-based reconstruction with WA-PLS (latitudinal bands that contain**
 674 **fewer than three grid cells are not shown).**

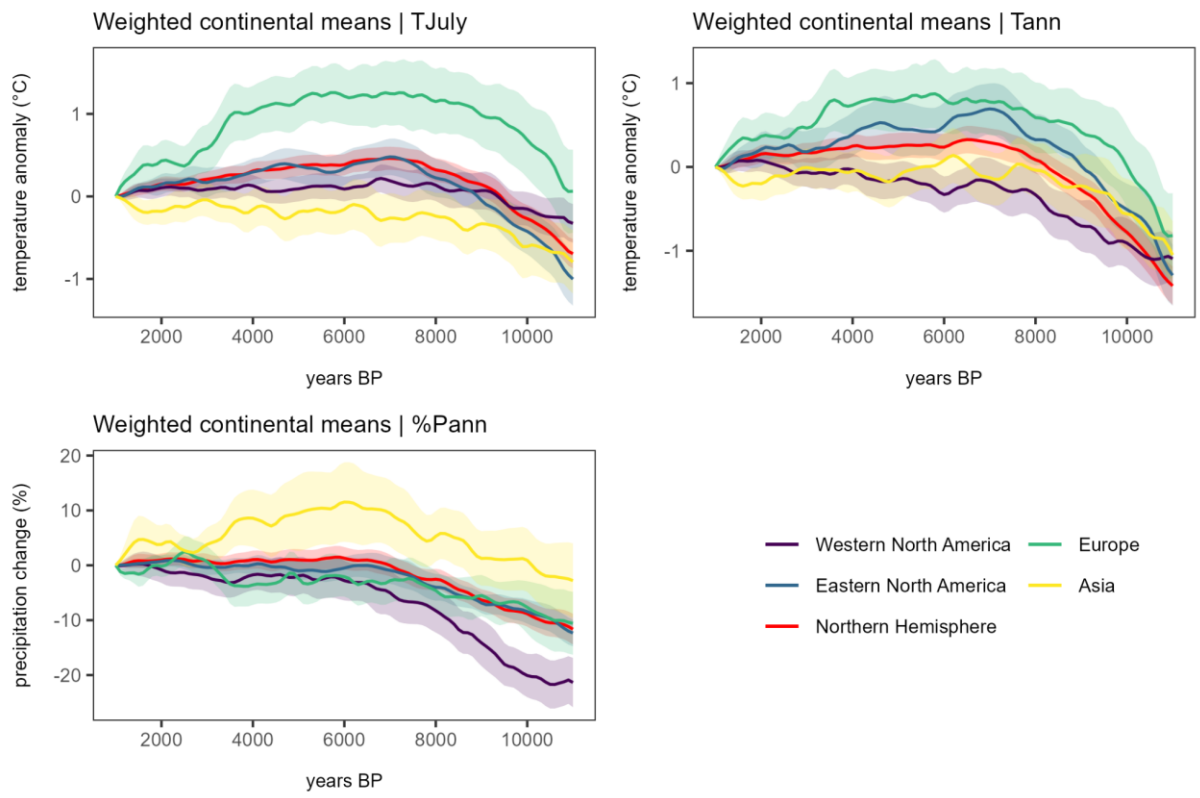
675



676

677 **Appendix Figure 7: Asian latitudinal mean curves with shaded standard errors for T_{July} , T_{ann} ,**
 678 **and $\%P_{ann}$ derived from pollen-based reconstruction with WA-PLS (latitudinal bands that contain**
 679 **fewer than three grid cells are not shown).**

680



681

682 **Appendix Figure 8: Weighted continental means with shaded standard errors for T_{July} , T_{ann} ,**
 683 **and $\%P_{ann}$ derived from pollen-based reconstruction with WA-PLS.**

684

685

686

687

688

689

690

691

692

693

694

695

696

697

698
699

Appendix Table 2. Significance values for zonal linear trends derived from a Monte-Carlo test comparison for mean July temperatures (T_{July}).

	<u>30-40°N</u>	<u>40-50°N</u>	<u>50-60°N</u>	<u>60-70°N</u>	<u>70-80°N</u>
<u>Western North America</u>	<u>30-40°N</u>	<u>p < 0.01</u>	<u>p < 0.01</u>	<u>p < 0.01</u>	<u>p < 0.01</u>
	<u>40-50°N</u>	<u>p < 0.01</u>	<u>p < 0.01</u>	<u>p < 0.01</u>	<u>p < 0.01</u>
	<u>50-60°N</u>	<u>p < 0.01</u>	<u>p < 0.01</u>	<u>p < 0.01</u>	<u>p < 0.01</u>
	<u>60-70°N</u>	<u>p < 0.01</u>	<u>p < 0.01</u>	<u>p < 0.01</u>	<u>p < 0.01</u>
	<u>70-80°N</u>	<u>p < 0.01</u>	<u>p < 0.01</u>	<u>p < 0.01</u>	<u>p < 0.01</u>
<u>Eastern North America</u>	<u>30-40°N</u>	<u>p < 0.01</u>	<u>p < 0.01</u>	<u>p < 0.01</u>	<u>p < 0.01</u>
	<u>40-50°N</u>	<u>p < 0.01</u>	<u>p < 0.01</u>	<u>p < 0.01</u>	<u>p < 0.01</u>
	<u>50-60°N</u>	<u>p < 0.01</u>	<u>p < 0.01</u>	<u>p < 0.01</u>	<u>p < 0.01</u>
	<u>60-70°N</u>	<u>p < 0.01</u>	<u>p < 0.01</u>	<u>p < 0.01</u>	<u>p < 0.01</u>
	<u>70-80°N</u>	<u>p < 0.01</u>	<u>p < 0.01</u>	<u>p < 0.01</u>	<u>p < 0.01</u>
<u>Europe</u>	<u>30-40°N</u>	<u>p < 0.01</u>	<u>p < 0.01</u>	<u>p < 0.01</u>	<u>p < 0.01</u>
	<u>40-50°N</u>	<u>p < 0.01</u>	<u>p < 0.01</u>	<u>p < 0.01</u>	<u>p < 0.01</u>
	<u>50-60°N</u>	<u>p < 0.01</u>	<u>p < 0.01</u>	<u>p < 0.01</u>	<u>p < 0.01</u>
	<u>60-70°N</u>	<u>p < 0.01</u>	<u>p < 0.01</u>	<u>p < 0.01</u>	<u>p < 0.01</u>
	<u>70-80°N</u>	<u>p < 0.01</u>	<u>p < 0.01</u>	<u>p < 0.01</u>	<u>p < 0.01</u>
<u>Asia</u>	<u>30-40°N</u>	<u>p < 0.01</u>	<u>p < 0.01</u>	<u>p < 0.01</u>	<u>p < 0.01</u>
	<u>40-50°N</u>	<u>p < 0.01</u>	<u>p < 0.01</u>	<u>p < 0.01</u>	<u>p < 0.01</u>
	<u>50-60°N</u>	<u>p < 0.01</u>	<u>p < 0.01</u>	<u>p < 0.01</u>	<u>p < 0.01</u>
	<u>60-70°N</u>	<u>p < 0.01</u>	<u>p < 0.01</u>	<u>p < 0.01</u>	<u>p < 0.01</u>
	<u>70-80°N</u>	<u>p < 0.01</u>	<u>p < 0.01</u>	<u>p < 0.01</u>	<u>p < 0.01</u>

700

701 **Appendix Table 3.** Significance values for zonal linear trends derived from a Monte-Carlo test
 702 comparison for mean annual temperatures (T_{ann}).

	<u>30-40°N</u>	<u>40-50°N</u>	<u>50-60°N</u>	<u>60-70°N</u>	<u>70-80°N</u>
<u>Western North America</u>	<u>30-40°N</u>	<u>$p < 0.01$</u>	<u>$p < 0.01$</u>	<u>$p < 0.01$</u>	<u>$p < 0.01$</u>
	<u>40-50°N</u>	<u>$p < 0.01$</u>	<u>$p < 0.01$</u>	<u>$p < 0.01$</u>	<u>$p < 0.01$</u>
	<u>50-60°N</u>	<u>$p < 0.01$</u>	<u>$p < 0.01$</u>	<u>$p < 0.01$</u>	<u>$p < 0.01$</u>
	<u>60-70°N</u>	<u>$p < 0.01$</u>	<u>$p < 0.01$</u>	<u>$p < 0.01$</u>	<u>$p < 0.01$</u>
	<u>70-80°N</u>	<u>$p < 0.01$</u>	<u>$p < 0.01$</u>	<u>$p < 0.01$</u>	<u>$p < 0.01$</u>
<u>Eastern North America</u>	<u>30-40°N</u>	<u>$p < 0.01$</u>	<u>$p < 0.01$</u>	<u>$p < 0.01$</u>	<u>$p < 0.01$</u>
	<u>40-50°N</u>	<u>$p < 0.01$</u>	<u>$p < 0.01$</u>	<u>$p < 0.01$</u>	<u>$p < 0.01$</u>
	<u>50-60°N</u>	<u>$p < 0.01$</u>	<u>$p < 0.01$</u>	<u>$p < 0.01$</u>	<u>$p < 0.01$</u>
	<u>60-70°N</u>	<u>$p < 0.01$</u>	<u>$p < 0.01$</u>	<u>$p < 0.01$</u>	<u>$p < 0.01$</u>
	<u>70-80°N</u>	<u>$p < 0.01$</u>	<u>$p < 0.01$</u>	<u>$p < 0.01$</u>	<u>$p < 0.01$</u>
<u>Europe</u>	<u>30-40°N</u>	<u>$p < 0.01$</u>	<u>$p < 0.01$</u>	<u>$p < 0.01$</u>	<u>$p < 0.01$</u>
	<u>40-50°N</u>	<u>$p < 0.01$</u>	<u>$p < 0.01$</u>	<u>$p < 0.01$</u>	<u>$p < 0.01$</u>
	<u>50-60°N</u>	<u>$p < 0.01$</u>	<u>$p < 0.01$</u>	<u>$p < 0.01$</u>	<u>$p < 0.01$</u>
	<u>60-70°N</u>	<u>$p < 0.01$</u>	<u>$p < 0.01$</u>	<u>$p < 0.01$</u>	<u>$p < 0.01$</u>
	<u>70-80°N</u>	<u>$p < 0.01$</u>	<u>$p < 0.01$</u>	<u>$p < 0.01$</u>	<u>$p < 0.01$</u>
<u>Asia</u>	<u>30-40°N</u>	<u>$p < 0.01$</u>	<u>$p < 0.01$</u>	<u>$p < 0.01$</u>	<u>$p < 0.01$</u>
	<u>40-50°N</u>	<u>$p < 0.01$</u>	<u>$p < 0.01$</u>	<u>$p < 0.01$</u>	<u>$p < 0.01$</u>
	<u>50-60°N</u>	<u>$p < 0.01$</u>	<u>$p < 0.01$</u>	<u>$p < 0.01$</u>	<u>$p < 0.01$</u>
	<u>60-70°N</u>	<u>$p < 0.01$</u>	<u>$p < 0.01$</u>	<u>$p < 0.01$</u>	<u>$p < 0.01$</u>
	<u>70-80°N</u>	<u>$p < 0.01$</u>	<u>$p < 0.01$</u>	<u>$p < 0.01$</u>	<u>$p < 0.01$</u>

703

704 **Appendix Table 4.** Significance values for zonal linear trends derived from a Monte-Carlo test
 705 comparison for annual precipitation (P_{ann}).

	<u>30-40°N</u>	<u>40-50°N</u>	<u>50-60°N</u>	<u>60-70°N</u>	<u>70-80°N</u>
<u>Western North America</u>	<u>30-40°N</u>	<u>$p < 0.01$</u>	<u>$p < 0.01$</u>	<u>$p < 0.01$</u>	<u>$p < 0.01$</u>
	<u>40-50°N</u>	<u>$p < 0.01$</u>	<u>$p < 0.01$</u>	<u>$p < 0.01$</u>	<u>$p < 0.01$</u>
	<u>50-60°N</u>	<u>$p < 0.01$</u>	<u>$p < 0.01$</u>	<u>$p < 0.01$</u>	<u>$p < 0.01$</u>
	<u>60-70°N</u>	<u>$p < 0.01$</u>	<u>$p < 0.01$</u>	<u>$p < 0.01$</u>	<u>$p < 0.01$</u>
	<u>70-80°N</u>	<u>0.06</u>	<u>$p < 0.01$</u>	<u>$p < 0.01$</u>	<u>$p < 0.01$</u>
<u>Eastern North America</u>	<u>30-40°N</u>	<u>$p < 0.01$</u>	<u>$p < 0.01$</u>	<u>$p < 0.01$</u>	<u>$p < 0.01$</u>
	<u>40-50°N</u>	<u>$p < 0.01$</u>	<u>$p < 0.01$</u>	<u>$p < 0.01$</u>	<u>$p < 0.01$</u>
	<u>50-60°N</u>	<u>$p < 0.01$</u>	<u>$p < 0.01$</u>	<u>$p < 0.01$</u>	<u>$p < 0.01$</u>
	<u>60-70°N</u>	<u>$p < 0.01$</u>	<u>$p < 0.01$</u>	<u>$p < 0.01$</u>	<u>$p < 0.01$</u>
	<u>70-80°N</u>	<u>$p < 0.01$</u>	<u>$p < 0.01$</u>	<u>$p < 0.01$</u>	<u>$p < 0.01$</u>
<u>Europe</u>	<u>30-40°N</u>	<u>$p < 0.01$</u>	<u>$p < 0.01$</u>	<u>$p < 0.01$</u>	<u>$p < 0.01$</u>
	<u>40-50°N</u>	<u>$p < 0.01$</u>	<u>$p < 0.01$</u>	<u>$p < 0.01$</u>	<u>$p < 0.01$</u>
	<u>50-60°N</u>	<u>$p < 0.01$</u>	<u>$p < 0.01$</u>	<u>$p < 0.01$</u>	<u>$p < 0.01$</u>
	<u>60-70°N</u>	<u>$p < 0.01$</u>	<u>$p < 0.01$</u>	<u>$p < 0.01$</u>	<u>$p < 0.01$</u>
	<u>70-80°N</u>	<u>$p < 0.01$</u>	<u>$p < 0.01$</u>	<u>$p < 0.01$</u>	<u>$p < 0.01$</u>
<u>Asia</u>	<u>30-40°N</u>	<u>0.08</u>	<u>$p < 0.01$</u>	<u>$p < 0.01$</u>	<u>0.76</u>
	<u>40-50°N</u>	<u>0.02</u>	<u>$p < 0.01$</u>	<u>$p < 0.01$</u>	<u>$p < 0.01$</u>
	<u>50-60°N</u>	<u>$p < 0.01$</u>	<u>$p < 0.01$</u>	<u>$p < 0.01$</u>	<u>$p < 0.01$</u>
	<u>60-70°N</u>	<u>$p < 0.01$</u>	<u>$p < 0.01$</u>	<u>$p < 0.01$</u>	<u>$p < 0.01$</u>
	<u>70-80°N</u>	<u>0.39</u>	<u>0.02</u>	<u>$p < 0.01$</u>	<u>$p < 0.01$</u>

706

707 **Appendix Table 5.** Significance values for continental means linear trends derived from a Monte-Carlo
 708 test comparison.

	<u>Western North</u>	<u>Eastern North</u>	<u>Europe</u>	<u>Asia</u>
	<u>America</u>	<u>America</u>		
T_{July}	<u>Western North</u>		<u>p < 0.01</u>	<u>p < 0.01</u>
	<u>America</u>		<u>p < 0.01</u>	<u>p < 0.01</u>
	<u>Eastern North</u>	<u>p < 0.01</u>		<u>p < 0.01</u>
	<u>America</u>	<u>p < 0.01</u>	<u>p < 0.01</u>	<u>p < 0.01</u>
	<u>Europe</u>	<u>p < 0.01</u>	<u>p < 0.01</u>	<u>p < 0.01</u>
	<u>Asia</u>	<u>p < 0.01</u>	<u>p < 0.01</u>	
T_{ann}	<u>Western North</u>		<u>p < 0.01</u>	<u>p < 0.01</u>
	<u>America</u>		<u>p < 0.01</u>	<u>p < 0.01</u>
	<u>Eastern North</u>	<u>p < 0.01</u>		<u>p < 0.01</u>
	<u>America</u>	<u>p < 0.01</u>	<u>p < 0.01</u>	<u>p < 0.01</u>
	<u>Europe</u>	<u>p < 0.01</u>	<u>p < 0.01</u>	<u>0.08</u>
	<u>Asia</u>	<u>p < 0.01</u>	<u>0.9</u>	
P_{ann}	<u>Western North</u>		<u>p < 0.01</u>	<u>p < 0.01</u>
	<u>America</u>		<u>p < 0.01</u>	<u>p < 0.01</u>
	<u>Eastern North</u>	<u>p < 0.01</u>		<u>p < 0.01</u>
	<u>America</u>	<u>p < 0.01</u>	<u>p < 0.01</u>	<u>p < 0.01</u>
	<u>Europe</u>	<u>p < 0.01</u>	<u>p < 0.01</u>	<u>p < 0.01</u>
	<u>Asia</u>	<u>p < 0.01</u>	<u>p < 0.01</u>	

709
 710 **Appendix Table 6.** Significance values for continental means compared to the Northern Hemispheric
 711 mean derived from a Monte-Carlo test comparison.

	<u>Western North</u>	<u>Eastern North</u>	<u>Europe</u>	<u>Asia</u>
	<u>America</u>	<u>America</u>		
T_{July}	<u>p < 0.01</u>	<u>p < 0.01</u>	<u>p < 0.01</u>	<u>p < 0.01</u>
T_{ann}	<u>p < 0.01</u>	<u>p < 0.01</u>	<u>p < 0.01</u>	<u>p < 0.01</u>
P_{ann}	<u>p < 0.01</u>	<u>p < 0.01</u>	<u>p < 0.01</u>	<u>p < 0.01</u>

713 **References**

- 714 [Andreev, A., Tarasov, P., Schwamborn, G., Ilyashuk, B., Ilyashuk, E., Bobrov, A., Klimanov, V., Rachold,](#)
715 [V., and Hubberten, H.-W.: Holocene paleoenvironmental records from Nikolay Lake, Lena River Delta,](#)
716 [Arctic Russia, *Palaeogeogr., Palaeoclim., Palaeoecol.*, 209, 197–217,](#)
717 <https://doi.org/10.1016/j.palaeo.2004.02.010>, 2004.
- 718 Bader, J., Jungclaus, J., Krivova, N., Lorenz, S., Maycock, A., Raddatz, T., Schmidt, H., Toohey, M.,
719 Wu, C.-J., and Claussen, M.: Global temperature modes shed light on the Holocene temperature
720 conundrum, *Nat. Commun.*, 11, 4726, <https://doi.org/10.1038/s41467-020-18478-6>, 2020.
- 721 Bakker, P., Rogozhina, I., Merkel, U., and Prange, M.: Hypersensitivity of glacial summer temperatures
722 in Siberia, *Clim. Past*, 16, 371–386, <https://doi.org/10.5194/cp-16-371-2020>, 2020.
- 723 Birks, H. J. B., Heiri, O., Seppä, H., and Bjune, A. E.: Strengths and Weaknesses of Quantitative Climate
724 Reconstructions Based on Late-Quaternary, *Open Ecol. J.*, 3,
725 <http://dx.doi.org/10.2174/1874213001003020068>, 2010.
- 726 Birks, H. J. B. and Simpson, G. L.: ‘Diatoms and pH reconstruction’ (1990) revisited, *J. Paleolimnol.*, 49,
727 363–371, <https://doi.org/10.1007/s10933-013-9697-7>, 2013.
- 728 [Blaauw, M. and Christen, J. A.: Flexible paleoclimate age-depth models using an autoregressive gamma](#)
729 [process, *Bayesian Anal.*, 6, 457–474, https://doi.org/10.1214/11-BA618](#), 2011.
- 730 Bova, S., Rosenthal, Y., Liu, Z., Godad, S. P., and Yan, M.: Seasonal origin of the thermal maxima at
731 the Holocene and the last interglacial, *Nature*, 589, 548–553, <https://doi.org/10.1038/s41586-020->
732 03155-x, 2021.
- 733 ~~ter Braak, C. J. F. and Juggins, S.: Weighted averaging partial least squares regression (WA-PLS): an~~
734 ~~improved method for reconstructing environmental variables from species assemblages, *Hydrobiologia*,~~
735 ~~269, 485–502, https://doi.org/10.1007/BF00028046~~, 1993.
- 736 Brierley, C. M., Zhao, A., Harrison, S. P., Braconnot, P., Williams, C. J. R., Thornalley, D. J. R., Shi, X.,
737 Peterschmitt, J.-Y., Ohgaito, R., Kaufman, D. S., Kageyama, M., Hargreaves, J. C., Erb, M. P., Emile-
738 Geay, J., D’Agostino, R., Chandan, D., Carré, M., Bartlein, P. J., Zheng, W., Zhang, Z., Zhang, Q., Yang,
739 H., Volodin, E. M., Tomas, R. A., Routson, C., Peltier, W. R., Otto-Bliesner, B., Morozova, P. A., McKay,
740 N. P., Lohmann, G., Legrande, A. N., Guo, C., Cao, J., Brady, E., Annan, J. D., and Abe-Ouchi, A.:
741 Large-scale features and evaluation of the PMIP4-CMIP6 midHolocene simulations, *Clim. Past*, 16,
742 1847–1872, <https://doi.org/10.5194/cp-16-1847-2020>, 2020.
- 743 [Brodzik, M. J., Billingsley, B., Haran, T., Raup, B., and Savoie, M. H.: EASE-Grid 2.0: Incremental but](#)
744 [Significant Improvements for Earth-Gridded Data Sets, *IJGI*, 1, 32–45,](#)
745 <https://doi.org/10.3390/ijgi1010032>, 2012.

- 746 Cao, X., Ni, J., Herzschuh, U., Wang, Y., and Zhao, Y.: A late Quaternary pollen dataset from eastern
747 continental Asia for vegetation and climate reconstructions: Set up and evaluation, *Rev. Palaeobot.*
748 *Palynol.*, 194, 21–37, <https://doi.org/10.1016/j.revpalbo.2013.02.003>, 2013.
- 749 Cao, X., Herzschuh, U., Telford, R. J., and Ni, J.: A modern pollen–climate dataset from China and
750 Mongolia: Assessing its potential for climate reconstruction, *Rev. Palaeobot. Palynol.*, 211, 87–96,
751 <https://doi.org/10.1016/j.revpalbo.2014.08.007>, 2014.
- 752 Cao, X., Tian, F., Dallmeyer, A., and Herzschuh, U.: Northern Hemisphere biome changes (>30°N) since
753 40 cal ka BP and their driving factors inferred from model-data comparisons, *Quat. Sci. Rev.*, 220, 291–
754 309, <https://doi.org/10.1016/j.quascirev.2019.07.034>, 2019.
- 755 Cao, X., Tian, F., Telford, R. J., Ni, J., Xu, Q., Chen, F., Liu, X., Stebich, M., Zhao, Y., and Herzschuh,
756 U.: Impacts of the spatial extent of pollen-climate calibration-set on the absolute values, range and
757 trends of reconstructed Holocene precipitation, *Quat. Sci. Rev.*, 178, 37–53,
758 <https://doi.org/10.1016/j.quascirev.2017.10.030>, 2017.
- 759 [Cartapanis, O., Jonkers, L., Moffa-Sanchez, P., Jaccard, S. L., and de Vernal, A.: Complex spatio-](https://doi.org/10.1038/s41467-022-33362-1)
760 [temporal structure of the Holocene Thermal Maximum, *Nat Commun*, 13, 5662,](https://doi.org/10.1038/s41467-022-33362-1)
761 <https://doi.org/10.1038/s41467-022-33362-1>, 2022.
- 762 Chang, E. K. M., Lee, S., and Swanson, K. L.: Storm Track Dynamics, *J. Clim.*, 15, 2163–2183,
763 [https://doi.org/10.1175/1520-0442\(2002\)015<02163:STD>2.0.CO;2](https://doi.org/10.1175/1520-0442(2002)015<02163:STD>2.0.CO;2), 2002.
- 764 Chen, F., Xu, Q., Chen, J., Birks, H. J. B., Liu, J., Zhang, S., Jin, L., An, C., Telford, R. J., Cao, X., Wang,
765 Z., Zhang, X., Selvaraj, K., Lu, H., Li, Y., Zheng, Z., Wang, H., Zhou, A., Dong, G., Zhang, J., Huang,
766 X., Bloemendal, J., and Rao, Z.: East Asian summer monsoon precipitation variability since the last
767 deglaciation, *Sci. Rep.*, 5, 11186, <https://doi.org/10.1038/srep11186>, 2015.
- 768 Chen, F., Chen, J., Huang, W., Chen, S., Huang, X., Jin, L., Jia, J., Zhang, X., An, C., Zhang, J., Zhao,
769 Y., Yu, Z., Zhang, R., Liu, J., Zhou, A., and Feng, S.: Westerlies Asia and monsoonal Asia:
770 Spatiotemporal differences in climate change and possible mechanisms on decadal to sub-orbital
771 timescales, *Earth Sci. Rev.*, 192, 337–354, <https://doi.org/10.1016/j.earscirev.2019.03.005>, 2019.
- 772 Chevalier, M., Davis, B. A. S., Heiri, O., Seppä, H., Chase, B. M., Gajewski, K., Lacourse, T., Telford,
773 R. J., Finsinger, W., Guiot, J., Köhl, N., Maezumi, S. Y., Tipton, J. R., Carter, V. A., Brussel, T., Phelps,
774 L. N., Dawson, A., Zanon, M., Vallé, F., Nolan, C., Mauri, A., de Vernal, A., Izumi, K., Holmström, L.,
775 Marsicek, J., Goring, S., Sommer, P. S., Chaput, M., and Kupriyanov, D.: Pollen-based climate
776 reconstruction techniques for late Quaternary studies, *Earth Sci. Rev.*, 210, 103384,
777 <https://doi.org/10.1016/j.earscirev.2020.103384>, 2020.

778 Chouinard, C. and Mareschal, J.-C.: Ground surface temperature history in southern Canada:
779 Temperatures at the base of the Laurentide ice sheet and during the Holocene, *Earth Planet. Sci. Lett.*,
780 277, 280–289, <https://doi.org/10.1016/j.epsl.2008.10.026>, 2009.

781 Cleator, S. F., Harrison, S. P., Nichols, N. K., Prentice, I. C., and Roulstone, I.: A new multivariable
782 benchmark for Last Glacial Maximum climate simulations, *Clim. Past*, 16, 699–712,
783 <https://doi.org/10.5194/cp-16-699-2020>, 2020.

784 Dallmeyer, A., Claussen, M., Lorenz, S. J., Sigl, M., Toohey, M., and Herzschuh, U.: Holocene
785 vegetation transitions and their climatic drivers in MPI-ESM1.2, *Clim. Past*, 17, 2481–2513,
786 <https://doi.org/10.5194/cp-17-2481-2021>, 2021.

787 [Dallmeyer, A., Kleinen, T., Claussen, M., Weitzel, N., Cao, X., and Herzschuh, U.: The deglacial forest](#)
788 [conundrum, *Nat Commun*, 13, 6035, <https://doi.org/10.1038/s41467-022-33646-6>, 2022.](#)

789 Davis, B. A. S., Brewer, S., Stevenson, A. C., and Guiot, J.: The temperature of Europe during the
790 Holocene reconstructed from pollen data, *Quat. Sci. Rev.*, 22, 1701–1716,
791 [https://doi.org/10.1016/S0277-3791\(03\)00173-2](https://doi.org/10.1016/S0277-3791(03)00173-2), 2003.

792 Davis, B. A. S., Chevalier, M., Sommer, P., Carter, V. A., Finsinger, W., Mauri, A., Phelps, L. N., Zanon,
793 M., Abegglen, R., Åkesson, C. M., Alba-Sánchez, F., Anderson, R. S., Antipina, T. G., Atanassova, J.
794 R., Beer, R., Belyanina, N. I., Blyakharchuk, T. A., Borisova, O. K., Bozilova, E., Bukreeva, G., Bunting,
795 M. J., Clò, E., Colombaroli, D., Combourieu-Nebout, N., Desprat, S., Di Rita, F., Djamali, M., Edwards,
796 K. J., Fall, P. L., Feurdean, A., Fletcher, W., Florenzano, A., Furlanetto, G., Gaceur, E., Galimov, A. T.,
797 Galka, M., García-Moreiras, I., Giesecke, T., Grindean, R., Guido, M. A., Gvozdeva, I. G., Herzschuh,
798 U., Hjelle, K. L., Ivanov, S., Jahns, S., Jankovska, V., Jiménez-Moreno, G., Karpińska-Kołaczek, M.,
799 Kitaba, I., Kołaczek, P., Lapteva, E. G., Latałowa, M., Lebreton, V., Leroy, S., Leydet, M., Lopatina, D.
800 A., López-Sáez, J. A., Lotter, A. F., Magri, D., Marinova, E., Matthias, I., Mavridou, A., Mercuri, A. M.,
801 Mesa-Fernández, J. M., Mikishin, Y. A., Milecka, K., Montanari, C., Morales-Molino, C., Mrotzek, A.,
802 Muñoz Sobrino, C., Naidina, O. D., Nakagawa, T., Nielsen, A. B., Novenko, E. Y., Panajiotidis, S.,
803 Panova, N. K., Papadopoulou, M., Pardoe, H. S., Pędziszewska, A., Petrenko, T. I., Ramos-Román, M.
804 J., Ravazzi, C., Rösch, M., Ryabogina, N., Sabariego Ruiz, S., Salonen, J. S., Sapelko, T. V., Schofield,
805 J. E., Seppä, H., Shumilovskikh, L., Stivrins, N., Stojakowits, P., Svobodova Svitavska, H., Święta-
806 Musznicka, J., Tantau, I., Tinner, W., Tobolski, K., Tonkov, S., Tsakiridou, M., et al.: The Eurasian
807 Modern Pollen Database (EMPD), version 2, *Earth Syst. Sci. Data*, 12, 2423–2445,
808 <https://doi.org/10.5194/essd-12-2423-2020>, 2020.

809 Dugerdil, L., Joannin, S., Peyron, O., Jouffroy-Bapicot, I., Vannièrre, B., Boldgiv, B., Unkelbach, J.,
810 Behling, H., and Ménot, G.: Climate reconstructions based on GDGT and pollen surface datasets from
811 Mongolia and Baikal area: calibrations and applicability to extremely cold–dry environments over the
812 Late Holocene, *Clim. Past*, 17, 1199–1226, <https://doi.org/10.5194/cp-17-1199-2021>, 2021.

813 Fick, S. E. and Hijmans, R. J.: WorldClim 2: new 1-km spatial resolution climate surfaces for global land
814 areas, *Int. J. Climatol.*, 37, 4302–4315, <https://doi.org/10.1002/joc.5086>, 2017.

815 Grimm, E. C., Lozano-García, S., Behling, H., and Markgraf, V.: Chapter 19 - Holocene Vegetation and
816 Climate Variability in the Americas, in: *Interhemispheric Climate Linkages*, edited by: Markgraf, V.,
817 Academic Press, San Diego, 325–370, <https://doi.org/10.1016/B978-012472670-3/50022-7>, 2001.

818 [Harrell, F. E. and Dupont, C.: Hmisc: Harrell Miscellaneous, R package version 5.0-1, https://cran.r-](https://cran.r-project.org/web/packages/Hmisc)
819 [project.org/web/packages/Hmisc, 2023.](https://cran.r-project.org/web/packages/Hmisc)

820 Harrison, S. P., Kutzbach, J. E., Liu, Z., Bartlein, P. J., Otto-Bliesner, B., Muhs, D., Prentice, I. C., and
821 Thompson, R. S.: Mid-Holocene climates of the Americas: a dynamical response to changed seasonality,
822 *Clim. Dyn.*, 20, 663–688, <https://doi.org/10.1007/s00382-002-0300-6>, 2003.

823 [Herzschuh, U.: Legacy of the Last Glacial on the present-day distribution of deciduous versus evergreen](https://doi.org/10.1111/geb.13018)
824 [boreal forests, *Global Ecology and Biogeography*, 29, 198-206, https://doi.org/10.1111/geb.13018,](https://doi.org/10.1111/geb.13018)
825 [2020.](https://doi.org/10.1111/geb.13018)

826 [Herzschuh, U., Tarasov, P., Wünnemann, B., and Hartmann, K.: Holocene vegetation and climate of](https://doi.org/10.1016/j.palaeo.2004.04.001)
827 [the Alashan Plateau, NW China, reconstructed from pollen data, *Palaeogeogr. Palaeoclimatol.*](https://doi.org/10.1016/j.palaeo.2004.04.001)
828 [Palaeoecol., 211, 1–17, https://doi.org/10.1016/j.palaeo.2004.04.001, 2004.](https://doi.org/10.1016/j.palaeo.2004.04.001)

829 [Herzschuh, U., Birks, H. J. B., Laepple, T., Andreev, A., Melles, M., and Brigham-Grette, J.: Glacial](https://doi.org/10.1038/ncomms11967)
830 [legacies on interglacial vegetation at the Pliocene-Pleistocene transition in NE Asia, *Nat Commun*, 7,](https://doi.org/10.1038/ncomms11967)
831 [11967, https://doi.org/10.1038/ncomms11967, 2016.](https://doi.org/10.1038/ncomms11967)

832 [Herzschuh, U., Cao, X., Laepple, T., Dallmeyer, A., Telford, R. J., Ni, J., Chen, F., Kong, Z., Liu, G., Liu,](https://doi.org/10.1038/s41467-019-09866-8)
833 [K.-B., Liu, X., Stebich, M., Tang, L., Tian, F., Wang, Y., Wischniewski, J., Xu, Q., Yan, S., Yang, Z., Yu,](https://doi.org/10.1038/s41467-019-09866-8)
834 [G., Zhang, Y., Zhao, Y., and Zheng, Z.: Position and orientation of the westerly jet determined Holocene](https://doi.org/10.1038/s41467-019-09866-8)
835 [rainfall patterns in China, *Nat. Commun.*, 10, 2376, https://doi.org/10.1038/s41467-019-09866-8, 2019.](https://doi.org/10.1038/s41467-019-09866-8)

836 Herzschuh, U., Böhmer, T., Li, C., and Cao, X.: Northern Hemisphere temperature and precipitation
837 reconstruction from taxonomically harmonized pollen data set with revised chronologies using WA-PLS
838 and MAT (LegacyClimate 1.0), PANGAEA, <https://doi.pangaea.de/10.1594/PANGAEA.930512>, 2021.

839 Herzschuh, U., Böhmer, T., Li, C., Chevalier, M., Dallmeyer, A., Cao, X., Bigelow, N. H., Nazarova, L.,
840 Novenko, E. Y., Park, J., Peyron, O., Rudaya, N. A., Schlütz, F., Shumilovskikh, L. S., Tarasov, P. E.,
841 Wang, Y., Wen, R., Xu, Q., and Zheng, Z.: LegacyClimate 1.0: A dataset of pollen-based climate
842 reconstructions from 2594 Northern Hemisphere sites covering the [last 30 ka and beyond](https://doi.org/10.5194/essd-2022-38)
843 [late Quaternary](https://doi.org/10.5194/essd-2022-38), *Earth Syst. Sci. Data*, 1–29, <https://doi.org/10.5194/essd-2022-38>, 2022a.

844 Herzschuh, U., Li, C., Böhmer, T., Postl, A. K., Heim, B., Andreev, A. A., Cao, X., Wiczorek, M., and
845 Ni, J.: LegacyPollen 1.0: [a taxonomically harmonized global late Quaternary pollen dataset of](https://doi.org/10.5194/essd-2022-38)

846 2831 records with standardized chronologies, *Earth Syst. Sci. Data*, **14**, 3213–3227,
847 <https://doi.org/10.5194/essd-14-3213-2022>, ~~*Sci. Data*, **1–25**, <https://doi.org/10.5194/essd-2022-37>,~~
848 2022b.

849 Hijmans, R. J., van Etten, J., Sumner, M., Cheng, J., Baston, D., Bevan, A., Bivand, R., Busetto, L.,
850 Canty, M., Fasoli, B., Forrest, D., Ghosh, A., Golicher, D., Gray, J., Greenberg, J. A., Hiemstra, P.,
851 Hingee, K., Ilich, A., Institute for Mathematics Applied Geosciences, Karney, C., Mattiuzzi, M., Mosher,
852 S., Naimi, B., Nowosad, J., Pebesma, E., Lamigueiro, O. P., Racine, E. B., Rowlingson, B., Shortridge,
853 A., Venables, B., and Wueest, R.: Raster: Geographic Data Analysis and Modeling, R package version
854 3.5-11, <https://cran.r-project.org/web/packages/raster>,
855 2021.

856 Jin, L., Chen, F., Morrill, C., Otto-Bliesner, B. L., and Rosenbloom, N.: Causes of early Holocene
857 desertification in arid central Asia, *Clim. Dyn.*, **38**, 1577–1591, [https://doi.org/10.1007/s00382-011-](https://doi.org/10.1007/s00382-011-1086-1)
858 1086-1, 2012.

859 Juggins, S.: Quantitative reconstructions in palaeolimnology: new paradigm or sick science?, *Quat. Sci.*
860 *Rev.*, **64**, 20–32, <https://doi.org/10.1016/j.quascirev.2012.12.014>, 2013.

861 Kaufman, D., McKay, N., Routson, C., Erb, M., Davis, B., Heiri, O., Jaccard, S., Tierney, J., Dätwyler,
862 C., Axford, Y., Brussel, T., Cartapanis, O., Chase, B., Dawson, A., de Vernal, A., Engels, S., Jonkers,
863 L., Marsicek, J., Moffa-Sánchez, P., Morrill, C., Orsi, A., Rehfeld, K., Saunders, K., Sommer, P. S.,
864 Thomas, E., Tonello, M., Tóth, M., Vachula, R., Andreev, A., Bertrand, S., Biskaborn, B., Bringué, M.,
865 Brooks, S., Caniupán, M., Chevalier, M., Cwynar, L., Emile-Geay, J., Fegyveresi, J., Feurdean, A.,
866 Finsinger, W., Fortin, M.-C., Foster, L., Fox, M., Gajewski, K., Grosjean, M., Hausmann, S., Heinrichs,
867 M., Holmes, N., Ilyashuk, B., Ilyashuk, E., Juggins, S., Khider, D., Koinig, K., Langdon, P., Larocque-
868 Tobler, I., Li, J., Lotter, A., Luoto, T., Mackay, A., Magyari, E., Malevich, S., Mark, B., Massferro, J.,
869 Montade, V., Nazarova, L., Novenko, E., Pařil, P., Pearson, E., Peros, M., Pienitz, R., Płóciennik, M.,
870 Porinchu, D., Potito, A., Rees, A., Reinemann, S., Roberts, S., Rolland, N., Salonen, S., Self, A., Seppä,
871 H., Shala, S., St-Jacques, J.-M., Stenni, B., Syrykh, L., Tarrats, P., Taylor, K., van den Bos, V., Velle,
872 G., Wahl, E., Walker, I., Wilmshurst, J., Zhang, E., and Zhilich, S.: A global database of Holocene
873 paleotemperature records, *Sci. Data*, **7**, 115, <https://doi.org/10.1038/s41597-020-0445-3>, 2020a.

874 Kaufman, D., McKay, N., Routson, C., Erb, M., Dätwyler, C., Sommer, P. S., Heiri, O., and Davis, B.:
875 Holocene global mean surface temperature, a multi-method reconstruction approach, *Sci. Data*, **7**, 201,
876 <https://doi.org/10.1038/s41597-020-0530-7>, 2020b.

877 [Kaufman, D. S. and Broadman, E.: Revisiting the Holocene global temperature conundrum, *Nature*,
878 **614**, 425–435, <https://doi.org/10.1038/s41586-022-05536-w>, 2023.](https://doi.org/10.1038/s41586-022-05536-w)

879 Kubota, Y., Tada, R., and Kimoto, K.: Changes in East Asian summer monsoon precipitation during the
880 Holocene deduced from a freshwater flux reconstruction of the Changjiang (Yangtze River) based on

881 the oxygen isotope mass balance in the northern East China Sea, *Clim. Past*, 11, 265–281,
882 <https://doi.org/10.5194/cp-11-265-2015>, 2015.

883 Kutzbach, J. E.: Monsoon Climate of the Early Holocene: Climate Experiment with the Earth's Orbital
884 Parameters for 9000 Years Ago, *Science*, <https://doi.org/10.1126/science.214.4516.59>, 1981.

885 Ladd, M., Way, R. G., and Viau, A. E.: The impact of using different modern climate data sets in pollen-
886 based paleoclimate reconstructions of North America, *Quat. Sci. Rev.*, 112, 78–85,
887 <https://doi.org/10.1016/j.quascirev.2015.01.020>, 2015.

888 [Leipe, C., Nakagawa, T., Gotanda, K., Müller, S., and Tarasov, P. E.: Late Quaternary vegetation and](#)
889 [climate dynamics at the northern limit of the East Asian summer monsoon and its regional and global-](#)
890 [scale controls, *Quat. Sci. Rev.*, 116, 57–71, <https://doi.org/10.1016/j.quascirev.2015.03.012>, 2015.](#)

891 Li, C., Postl, A. K., Böhmer, T., Cao, X., Dolman, A. M., and Herzsuh, U.: Harmonized chronologies
892 of a global late Quaternary pollen dataset (LegacyAge 1.0), *Earth Syst. Sci. Data*, 14, 1331–1343,
893 <https://doi.org/10.5194/essd-14-1331-2022>, 2022.

894 Li, J., Wang, N., Dodson, J., Yan, H., Zhang, X., Jia, P. W., and Seppä, H.: Holocene negative coupling
895 of summer temperature and moisture availability over southeastern arid Central Asia, *Clim. Dyn.*, 55,
896 1187–1208, <https://doi.org/10.1007/s00382-020-05319-x>, 2020.

897 Liu, Z., Wen, X., Brady, E. C., Otto-Bliesner, B., Yu, G., Lu, H., Cheng, H., Wang, Y., Zheng, W., Ding,
898 Y., Edwards, R. L., Cheng, J., Liu, W., and Yang, H.: Chinese cave records and the East Asia Summer
899 Monsoon, *Quat. Sci. Rev.*, 83, 115–128, <https://doi.org/10.1016/j.quascirev.2013.10.021>, 2014a.

900 Liu, Z., Yoshimura, K., Bowen, G. J., Buening, N. H., Risi, C., Welker, J. M., and Yuan, F.: Paired
901 oxygen isotope records reveal modern North American atmospheric dynamics during the Holocene, *Nat.*
902 *Commun.*, 5, 3701, <https://doi.org/10.1038/ncomms4701>, 2014b.

903 Liu, Z., Zhu, J., Rosenthal, Y., Zhang, X., Otto-Bliesner, B. L., Timmermann, A., Smith, R. S., Lohmann,
904 G., Zheng, W., and Timm, O. E.: The Holocene temperature conundrum, *PNAS*, 111, E3501–E3505,
905 <https://doi.org/10.1073/pnas.1407229111>, 2014c.

906 Lohmann, G., Wagner, A., and Prange, M.: Resolution of the atmospheric model matters for the
907 Northern Hemisphere Mid-Holocene climate, *Dyn. Atmospheres Oceans*, 93, 101206,
908 <https://doi.org/10.1016/j.dynatmoce.2021.101206>, 2021.

909 Marcott, S. A., Shakun, J. D., Clark, P. U., and Mix, A. C.: A Reconstruction of Regional and Global
910 Temperature for the Past 11,300 Years, *Science*, <https://doi.org/10.1126/science.1228026>, 2013.

- 911 Marsicek, J., Shuman, B. N., Bartlein, P. J., Shafer, S. L., and Brewer, S.: Reconciling divergent trends
912 and millennial variations in Holocene temperatures, *Nature*, 554, 92–96,
913 <https://doi.org/10.1038/nature25464>, 2018.
- 914 Mauri, A., Davis, B. a. S., Collins, P. M., and Kaplan, J. O.: The influence of atmospheric circulation on
915 the mid-Holocene climate of Europe: a data–model comparison, *Clim. Past*, 10, 1925–1938,
916 <https://doi.org/10.5194/cp-10-1925-2014>, 2014.
- 917 Mauri, A., Davis, B. A. S., Collins, P. M., and Kaplan, J. O.: The climate of Europe during the Holocene:
918 a gridded pollen-based reconstruction and its multi-proxy evaluation, *Quat. Sci. Rev.*, 112, 109–127,
919 <https://doi.org/10.1016/j.quascirev.2015.01.013>, 2015.
- 920 McKay, N. P., Kaufman, D. S., Routson, C. C., Erb, M. P., and Zander, P. D.: The Onset and Rate of
921 Holocene Neoglacial Cooling in the Arctic, *Geophys. Res. Lett.*, 45, 12,487–12,496,
922 <https://doi.org/10.1029/2018GL079773>, 2018.
- 923 [Melles, M., Brigham-Grette, J., Minyuk, P.S., Nowaczyk, N.R., Wennrich, V., DeConto, R.M., Anderson,](#)
924 [P.M., Andreev, A.A., Coletti, A., Cook, T.L., Haltia-Hovi, E., Kukkonen, M., Lozhkin, A.V., Rosén, P.,](#)
925 [Tarasov, P., Vogel, H., and Wagner, B.: 2.8 Million years of Arctic climate change from Lake El'gygytgyn,](#)
926 [NE Russia, *Science*, 337, 315–320, <https://www.science.org/doi/10.1126/science.1222135>, 2012.](#)
- 927 [Nakagawa, T., Tarasov, P. E., Nishida, K., Gotanda, K., and Yasuda, Y.: Quantitative pollen-based](#)
928 [climate reconstruction in central Japan: application to surface and Late Quaternary spectra, *Quat. Sci.*](#)
929 [*Rev.*, 21, 2099–2113, \[https://doi.org/10.1016/S0277-3791\\(02\\)00014-8\]\(https://doi.org/10.1016/S0277-3791\(02\)00014-8\), 2002.](#)
- 930 Nolan, C., Tipton, J., Booth, R. K., Hooten, M. B., and Jackson, S. T.: Comparing and improving methods
931 for reconstructing peatland water-table depth from testate amoebae, *Holocene*, 29, 1350–1361,
932 <https://doi.org/10.1177/0959683619846969>, 2019.
- 933 Osman, M. B., Tierney, J. E., Zhu, J., Tardif, R., Hakim, G. J., King, J., and Poulsen, C. J.: Globally
934 resolved surface temperatures since the Last Glacial Maximum, *Nature*, 599, 239–244,
935 <https://doi.org/10.1038/s41586-021-03984-4>, 2021.
- 936 R Core Team: R: A language and environment for statistical computing, R Foundation for Statistical
937 Computing, Vienna, Austria, <https://www.r-project.org/>, 2020.
- 938 Renssen, H., Seppä, H., Heiri, O., Roche, D. M., Goosse, H., and Fichetfot, T.: The spatial and temporal
939 complexity of the Holocene thermal maximum, *Nat. Geosci.*, 2, 411–414,
940 <https://doi.org/10.1038/ngeo513>, 2009.
- 941 Renssen, H., Seppä, H., Crosta, X., Goosse, H., and Roche, D. M.: Global characterization of the
942 Holocene Thermal Maximum, *Quat. Sci. Rev.*, 48, 7–19,
943 <https://doi.org/10.1016/j.quascirev.2012.05.022>, 2012.

- 944 Reschke, M., Kunz, T., and Laepple, T.: Comparing methods for analysing time scale dependent
945 correlations in irregularly sampled time series data, *Comput. Geosci.*, 123, 65–72,
946 <https://doi.org/10.1016/j.cageo.2018.11.009>, 2019.
- 947 Rolandone, F., Mareschal, J.-C., and Jaupart, C.: Temperatures at the base of the Laurentide Ice Sheet
948 inferred from borehole temperature data, *Geophys. Res. Lett.*, 30,
949 <https://doi.org/10.1029/2003GL018046>, 2003.
- 950 Routson, C. C., McKay, N. P., Kaufman, D. S., Erb, M. P., Goosse, H., Shuman, B. N., Rodysill, J. R.,
951 and Ault, T.: Mid-latitude net precipitation decreased with Arctic warming during the Holocene, *Nature*,
952 568, 83–87, <https://doi.org/10.1038/s41586-019-1060-3>, 2019.
- 953 Routson, C. C., Kaufman, D. S., McKay, N. P., Erb, M. P., Arcusa, S. H., Brown, K. J., Kirby, M. E.,
954 Marsicek, J. P., Anderson, R. S., Jiménez-Moreno, G., Rodysill, J. R., Lachniet, M. S., Fritz, S. C.,
955 Bennett, J. R., Goman, M. F., Metcalfe, S. E., Galloway, J. M., Schoups, G., Wahl, D. B., Morris, J. L.,
956 Staines-Urías, F., Dawson, A., Shuman, B. N., Gavin, D. G., Munroe, J. S., and Cumming, B. F.: A
957 multiproxy database of western North American Holocene paleoclimate records, *Earth Syst. Sci. Data*,
958 13, 1613–1632, <https://doi.org/10.5194/essd-13-1613-2021>, 2021.
- 959 Salonen, J. S., Korpela, M., Williams, J. W., and Luoto, M.: Machine-learning based reconstructions of
960 primary and secondary climate variables from North American and European fossil pollen data, *Sci.*
961 *Rep.*, 9, 15805, <https://doi.org/10.1038/s41598-019-52293-4>, 2019.
- 962 Seager, R., Neelin, D., Simpson, I., Liu, H., Henderson, N., Shaw, T., Kushnir, Y., Ting, M., and Cook,
963 B.: Dynamical and Thermodynamical Causes of Large-Scale Changes in the Hydrological Cycle over
964 North America in Response to Global Warming, *J. Clim.*, 27, 7921–7948, <https://doi.org/10.1175/JCLI->
965 [D-14-00153.1](https://doi.org/10.1175/JCLI-D-14-00153.1), 2014.
- 966 Shin, S.-I., Sardeshmukh, P. D., Webb, R. S., Oglesby, R. J., and Barsugli, J. J.: Understanding the
967 Mid-Holocene Climate, *J. Clim.*, 19, 2801–2817, <https://doi.org/10.1175/JCLI3733.1>, 2006.
- 968 Simpson, G. L.: Analogue Methods in Palaeolimnology, in: *Tracking Environmental Change Using Lake*
969 *Sediments*, vol. 5: Data Handling and Numerical Techniques, edited by: Birks, H. J. B., Lotter, A. F.,
970 Juggins, S., and Smol, J. P., Springer Netherlands, Dordrecht, 495–522, <https://doi.org/10.1007/978->
971 [94-007-2745-8_15](https://doi.org/10.1007/978-94-007-2745-8_15), 2012.
- 972 [Stebich, M., Rehfeld, K., Schlütz, F., Tarasov, P. E., Liu, J., and Mingram, J.: Holocene vegetation and](#)
973 [climate dynamics of NE China based on the pollen record from Sihailongwan Maar Lake, *Quat. Sci.*](#)
974 [Rev., 124, 275–289, <https://doi.org/10.1016/j.quascirev.2015.07.021>, 2015.](#)

- 975 [Tarasov, P. E., Bezrukova, E. V., and Krivonogov, S. K.: Late Glacial and Holocene changes in](#)
976 [vegetation cover and climate in southern Siberia derived from a 15 kyr long pollen record from Lake](#)
977 [Kotokel, *Clim. Past*, 2009.](#)
- 978 Tarasov, P. E., Nakagawa, T., Demske, D., Österle, H., Igarashi, Y., Kitagawa, J., Mokhova, L.,
979 Bazarova, V., Okuda, M., Gotanda, K., Miyoshi, N., Fujiki, T., Takemura, K., Yonenobu, H., and Fleck,
980 A.: Progress in the reconstruction of Quaternary climate dynamics in the Northwest Pacific: A new
981 modern analogue reference dataset and its application to the 430-kyr pollen record from Lake Biwa,
982 *Earth Sci. Rev.*, 108, 64–79, <https://doi.org/10.1016/j.earscirev.2011.06.002>, 2011.
- 983 [Tarasov, P. E., Müller, S., Zech, M., Andreeva, D., Diekmann, B., and Leipe, C.: Last glacial vegetation](#)
984 [reconstructions in the extreme-continental eastern Asia: Potentials of pollen and n-alkane biomarker](#)
985 [analyses, *Quat. Int.*, 290–291, 253–263, <https://doi.org/10.1016/j.quaint.2012.04.007>, 2013.](#)
- 986 Telford, R. J. and Birks, H. J. B.: A novel method for assessing the statistical significance of quantitative
987 reconstructions inferred from biotic assemblages, *Quat. Sci. Rev.*, 30, 1272–1278,
988 <https://doi.org/10.1016/j.quascirev.2011.03.002>, 2011.
- 989 [ter Braak, C. J. F. and Juggins, S.: Weighted averaging partial least squares regression \(WA-PLS\): an](#)
990 [improved method for reconstructing environmental variables from species assemblages, *Hydrobiologia*,](#)
991 [269, 485–502, <https://doi.org/10.1007/BF00028046>, 1993.](#)
- 992 Trenberth, K. E.: Changes in precipitation with climate change, *Clim. Res.*, 47, 123–138,
993 <https://doi.org/10.3354/cr00953>, 2011.
- 994 Wang, N., Jiang, D., and Lang, X.: Mechanisms for Spatially Inhomogeneous Changes in East Asian
995 Summer Monsoon Precipitation during the Mid-Holocene, *J. Clim.*, 33, 2945–2965,
996 <https://doi.org/10.1175/JCLI-D-19-0565.1>, 2020.
- 997 Wang, Y., Liu, X., and Herzschuh, U.: Asynchronous evolution of the Indian and East Asian Summer
998 Monsoon indicated by Holocene moisture patterns in monsoonal central Asia, *Earth Sci. Rev.*, 103, 135–
999 153, <https://doi.org/10.1016/j.earscirev.2010.09.004>, 2010.
- 1000 Wang, Y., Bekeschus, B., Handorf, D., Liu, X., Dallmeyer, A., and Herzschuh, U.: Coherent tropical-
1001 subtropical Holocene see-saw moisture patterns in the Eastern Hemisphere monsoon systems, *Quat.*
1002 *Sci. Rev.*, 169, 231–242, <https://doi.org/10.1016/j.quascirev.2017.06.006>, 2017.
- 1003 Whitmore, J., Gajewski, K., Sawada, M., Williams, J. W., Shuman, B., Bartlein, P. J., Minckley, T., Viau,
1004 A. E., Webb, T., Shafer, S., Anderson, P., and Brubaker, L.: Modern pollen data from North America
1005 and Greenland for multi-scale paleoenvironmental applications, *Quat. Sci. Rev.*, 24, 1828–1848,
1006 <https://doi.org/10.1016/j.quascirev.2005.03.005>, 2005.

- 1007 Williams, J. W., [Grimm, E. C., Blois, J. L., Charles, D. F., Davis, E. B., Goring, S. J., Graham, R. W.,](#)
1008 [Smith, A. J., Anderson, M., Arroyo-Cabrales, J., Ashworth, A. C., Betancourt, J. L., Bills, B. W., Booth,](#)
1009 [R. K., Buckland, P. I., Curry, B. B., Giesecke, T., Jackson, S. T., Latorre, C., Nichols, J., Purdum, T.,](#)
1010 [Roth, R. E., Stryker, M., and Takahara, H.: The Neotoma Paleocology Database, a multiproxy,](#)
1011 [international, community-curated data resource, *Quat. Res.*, 89, 156–177,](#)
1012 <https://doi.org/10.1017/qua.2017.105>, 2018.
- 1013 [Williams, J. W.,](#) Webb III, T., Richard, P. H., and Newby, P.: Late Quaternary biomes of Canada and the
1014 eastern United States, *J. Biogeogr.*, 27, 585–607, <https://doi.org/10.1046/j.1365-2699.2000.00428.x>,
1015 2000.
- 1016 Xu, C., Yan, M., Ning, L., and Liu, J.: Summer Westerly Jet in Northern Hemisphere during the Mid-
1017 Holocene: A Multi-Model Study, *Atmos.*, 11, 1193, <https://doi.org/10.3390/atmos11111193>, 2020.
- 1018 [Zanon, M., Davis, B. A. S., Marquer, L., Brewer, S., and Kaplan, J. O.: European Forest Cover During](#)
1019 [the Past 12,000 Years: A Palynological Reconstruction Based on Modern Analogs and Remote Sensing,](#)
1020 [Front. Plant Sci., 9, 253, <https://doi.org/10.3389/fpls.2018.00253>, 2018.](#)
- 1021 Zhang, J., Chen, F., Holmes, J. A., Li, H., Guo, X., Wang, J., Li, S., Lü, Y., Zhao, Y., and Qiang, M.:
1022 Holocene monsoon climate documented by oxygen and carbon isotopes from lake sediments and peat
1023 bogs in China: a review and synthesis, *Quat. Sci. Rev.*, 30, 1973–1987,
1024 <https://doi.org/10.1016/j.quascirev.2011.04.023>, 2011.
- 1025 Zhang, Y., Renssen, H., and Seppä, H.: Effects of melting ice sheets and orbital forcing on the early
1026 Holocene warming in the extratropical Northern Hemisphere, *Clim. Past*, 12, 1119–1135,
1027 <https://doi.org/10.5194/cp-12-1119-2016>, 2016.
- 1028 Zhang, Z., Liu, J., Chen, J., Chen, S., Shen, Z., Chen, J., Liu, X., Wu, D., Sheng, Y., and Chen, F.:
1029 Holocene climatic optimum in the East Asian monsoon region of China defined by climatic stability, *Earth*
1030 *Sci. Rev.*, 212, 103450, <https://doi.org/10.1016/j.earscirev.2020.103450>, 2021.
- 1031 Zheng, W., Wu, B., He, J., and Yu, Y.: The East Asian Summer Monsoon at mid-Holocene: results from
1032 PMIP3 simulations, *Clim. Past*, 9, 453–466, <https://doi.org/10.5194/cp-9-453-2013>, 2013.
- 1033 Zhou, P., Shi, Z., Li, X., and Zhou, W.: Response of Westerly Jet Over the Northern Hemisphere to
1034 Astronomical Insolation During the Holocene, *Front. Earth Sci.*, 8,
1035 <https://doi.org/10.3389/feart.2020.00282>, 2020.